© 2018. Published by The Company of Biologists Ltd | Journal of Cell Science (2018) 131, jcs206995. doi:10.1242/jcs.206995

REVIEW

ARTICLE SERIES: IMAGING

Molecular mobility and activity in an intravital imaging setting – implications for cancer progression and targeting

Max Nobis*, Sean C. Warren*, Morghan C. Lucas, Kendelle J. Murphy, David Herrmann‡ and Paul Timpson‡

ABSTRACT

Molecular mobility, localisation and spatiotemporal activity are at the core of cell biological processes and deregulation of these dynamic events can underpin disease development and progression. Recent advances in intravital imaging techniques in mice are providing new avenues to study real-time molecular behaviour in intact tissues within a live organism and to gain exciting insights into the intricate regulation of live cell biology at the microscale level. The monitoring of fluorescently labelled proteins and agents can be combined with autofluorescent properties of the microenvironment to provide a comprehensive snapshot of *in vivo* cell biology. In this Review, we summarise recent intravital microscopy approaches in mice, in processes ranging from normal development and homeostasis to disease progression and treatment in cancer, where we emphasise the utility of intravital imaging to observe dynamic and transient events *in vivo*. We also highlight the recent integration of advanced subcellular imaging techniques into the intravital imaging pipeline, which can provide in-depth biological information beyond the single-cell level. We conclude with an outlook of ongoing developments in intravital microscopy towards imaging in humans, as well as provide an overview of the challenges the intravital imaging community currently faces and outline potential ways for overcoming these hurdles.

KEY WORDS: Intravital imaging, Subcellular imaging, FRAP, FRET, Biosensors, Cancer, Immune cells, Imaging software, Invasion and metastasis

Introduction

Intravital or *in vivo* microscopy (IVM) has emerged as a powerful technique for the anatomical and functional mapping of cell biology in live mice from the subcellular level to whole-body approaches (reviewed in Conway et al., 2014; Ellenbroek and van Rheenen, 2014; Vennin et al., 2016). The discovery of fluorescent proteins, such as green fluorescent protein (GFP) and related variants (Chalfie et al., 1994; Giepmans et al., 2006; Miyawaki et al., 1997; Prasher et al., 1992), and their introduction into mice by genetic engineering has opened exciting opportunities to track live cell biology and molecular dynamics *in vivo*. Combined IVM of fluorescent proteins with other fluorescently tagged probes, such as antibodies, drugs or nanoparticles, while also exploring the inherent or autofluorescent properties of endogenous compounds, such as extracellular matrix (ECM) or metabolites (see Table 1 for further detail) can provide a comprehensive biological insight into live animals with an improved fidelity compared with cell and tissue-culture models. Furthermore, the use of multiphoton microscopy with pulsed infrared lasers provides key advantages for IVM as this can significantly extend the imaging depths owing to the reduced absorption and scattering at longer excitation wavelengths, while providing strong optical sectioning. This is essential for imaging thick samples, without the need for a confocal pinhole, thereby reducing the effect of sample aberration on the image quality relative to confocal microscopy. The relative advantages of different microscope platforms are discussed in detail elsewhere (Follain et al., 2017; Pantazis and Supatto, 2014; Timpson et al., 2011).

In recent years, the promise of IVM has been vividly realised, moving from proof-of-concept studies to providing critical quantitative insights into biological processes, which would be impossible using *in vitro* studies. In this Review, we discuss recent advances in IVM in mice, highlighting intravital applications to study development and tissue homeostasis, along with cancer aetiology and treatment. For IVM applications in other areas of biology, such as neuroscience or immunology, the reader is referred to excellent recent reviews (Osswald and Winkler, 2013; Secklehner et al., 2017). We also provide a summary of the emerging use of more advanced, subcellular imaging technologies in IVM and an overview of imaging applications in humans, while concluding with a discussion on the challenges and bottlenecks faced in IVM.

IVM of live tissues upon surgical exposure

IVM in living mice poses several challenges that need to be considered; the first is tissue accessibility. To overcome this challenge for short-term and medium-term imaging, the tissue of interest can be surgically exposed, while preserving its structure, connectivity and perfusion in the anaesthetised mouse. For example, IVM of lipid droplets in epithelial cells of a surgically exposed lactating mammary gland highlighted the fate of lipid droplets from their synthesis in the endoplasmic reticulum to secretion at the apical plasma membrane in a live mouse (Fig. 1A; Masedunskas et al., 2017). Furthermore, IVM in surgically exposed tissues was used to characterise the role of the actomyosin cytoskeleton during exocytosis in the salivary gland (Milberg et al., 2017), to probe secretion and paracellular transport in the liver (Porat-Shliom et al., 2016) and to visualise T- and B-cell interactions in the germinal centre of intact lymph nodes (Xu et al., 2013a).

Some IVM approaches do not require surgical exposure of the tissue of interest. For example, live cell imaging in the retina was recently performed to observe dynamic radial infiltration patterns of immune cells in a mouse model of autoimmune retinal inflammation (Bremer et al., 2016). The auricular skin of the ear provides another easily accessible site to extract valuable *in vivo* cell

The Garvan Institute of Medical Research and The Kinghorn Cancer Centre, Cancer Division, St. Vincent's Clinical School, Faculty of Medicine, University of New South Wales, Sydney, NSW 2010, Australia.
*These authors contributed equally to this work.

‡Authors for correspondence (d.herrmann@garvan.org.au; p.timpson@garvan.org.au)

D.H., 0000-0002-9514-7501; P.T., 0000-0002-5514-7080

Journal of Cell Science (2018) 131, jcs206995. doi:10.1242/jcs.206995

Box 1. Subcellular imaging techniques

Fluorescence recovery after photobleaching (FRAP)

Fluorescence recovery inside a bleached region is monitored over time (Fig. 3A). Incomplete fluorescence recovery indicates partial immobilisation of the bleached molecule (immobile fraction and mobile fraction, Fig. 3B, graph (Fritzsche and Charras, 2015). FRAP has been used to characterise protein movement (de Beco et al., 2009; Goehring et al., 2010; Renz and Langowski, 2008), protein–protein interaction (Dunham et al., 2004), nuclear export (Wagner et al., 2004), signal transduction (Khait et al., 2016), focal adhesion turn-over (Kumar et al., 2016), cell–cell junction dynamics (Verma et al., 2012; Yamada et al., 2005) or gap junction function via 'gap-FRAP' (Abbaci et al., 2007; Farnsworth et al., 2014).

Fluorescence loss in photobleaching (FLIP)

Loss of fluorescence in regions adjacent to the bleached region is recorded (Fig. 3C,D). Combination of FRAP and FLIP can complement each other and reinforce the changes in molecular dynamics observed (Bolognesi et al., 2016; Erami et al., 2016; Jusu et al., 2017; Le Devedec et al., 2012).

Fluorescence resonance energy transfer (FRET)

Emission of a donor fluorophore excites the acceptor fluorophore depending on their spectral overlap, proximity and alignment to each other [Fig. 4A, reviewed in Piston and Kremers (2007)]. FRET efficiency can be measured by ratiometric or FLIM imaging. Ratiometric FRET is faster to perform because it records both the donor and acceptor fluorescence but may require further corrections to take into account potential cross-excitation of both donor and acceptor or spectral bleedthrough. FLIM-FRET measures the inherent fluorescence lifetime of the donor fluorophore, which is reduced in the presence of FRET. FLIM can provide a quantitative readout of FRET activity and, because it uses only the donor emission, is less sensitive to wavelength-dependent scattering and absorption from tissue. For further FRET imaging methods and analyses the reader is referred to other recent articles (Conway et al., 2017; Pietraszewska-Bogiel and Gadella, 2011; Radbruch et al., 2015; Warren et al., 2013).

Fluorescence lifetime imaging microscopy (FLIM)

Quantification of inherent fluorescence lifetime of a fluorophore as an exponential decay rate. The fluorescence lifetime is the time a fluorophore spends in the excited state before emitting a photon and returning to the ground state (Huck et al., 2016; Kalinina et al., 2016; Stringari et al., 2012; Walsh et al., 2013; Wang et al., 2017).

Intramolecular FRET biosensors

Donor and acceptor fluorophores with linker in between that can be altered by kinases, phosphatases, proteases or protein interaction (Fig. 4A). FRET efficacy serves as a readout of protein or signalling pathway activity (Fig. 4B; Conway et al., 2014, 2017; Newman et al., 2011). Applications in cell proliferation (Harvey et al., 2008; Mochizuki et al., 2001), survival (Onuki et al., 2002; Tyas et al., 2000), signalling (Shih and Qi, 2017; Weitsman et al., 2016), immune cell activity (Choi and Mitchison, 2013; Li et al., 2016b), metabolism (Fehr et al., 2003; Imamura et al., 2009; Mächler et al., 2016; Okumoto et al., 2005) or migration (Seong et al., 2011; Wang et al., 2005) with a recent move to generate GEMMs of FRET biosensors for high-fidelity intravital imaging (Johnsson et al., 2014; Kamioka et al., 2012; Mukherjee et al., 2016; Nobis et al., 2017).

biology without the need for surgical intervention. Here, Li et al. (2016a) characterised how neutrophils take up fluorescent immune complexes and transmigrate with their cargo across the endothelium into the interstitium (Fig. 1B). Similarly, intravital photoconversion of the fluorescent protein Kikume, whose fluorescence irreversibly changes from green to red upon excitation with ultraviolet or violet light, was used to delineate pathways of Kikume-expressing neutrophil migration and response to pathogen introduction (Hampton et al., 2015). Such novel insights into neutrophil dynamics are important, considering that neutrophil recruitment has been shown to have a role in injury and diseases, such as infection or cancer progression, as well as their treatment (Hind et al., 2016; Powell et al., 2017; Steele et al., 2016).

Optical imaging of *in vivo* cell biology through imaging windows

Surgical insertion of optical imaging windows adjacent to an organ of interest allows the transient stabilisation of surgically exposed tissues and repeated long-term imaging of live tissue in the anaesthetised mouse (Bochner et al., 2015; Kedrin et al., 2008; Nobis et al., 2017; Ritsma et al., 2014, 2012, 2013b; Rodriguez-Tirado et al., 2016; Tabuchi et al., 2008). For instance, IVM of megakaryocytes and platelets in lung, liver, spleen and bone marrow through windows in fluorescent, genetically engineered mouse models (GEMMs) revealed that the lungs are a major site of platelet production and contain a pool of hematopoietic progenitors (Fig. 1C; Lefrançais et al., 2017). Similarly, intravital lung imaging of fluorescent antibody-labelled immune cell populations was used to characterise the *in vivo* recruitment dynamics of invariant natural killer T-cells, neutrophils and dendritic cells (Thanabalasuriar et al., 2016).

Cranial windows have been used to describe a detailed pathway that cells use to arrive and transmigrate into bone marrow sinusoids during homing (Bixel et al., 2017) and to track the fate and behaviour of transplanted bone marrow cells in the native bone microenvironment (Le et al., 2017). Other window approaches are specifically suited for surgical insertion at the cervical, thoracic or lumbar level along the spinal cord for IVM approaches in the live spinal cord microenvironment during tissue homeostasis or inflammation (Bartholomäus et al., 2009; Davalos et al., 2008; Haghayegh Jahromi et al., 2017; Kim et al., 2010; Odoardi et al., 2007; Yang et al., 2017; Zenaro et al., 2013).

Longitudinal tracking through imaging windows has also revealed novel insights into the positioning, maintenance and plasticity of mammary and intestinal stem cells (Fig. 1D; Ritsma et al., 2014; Scheele et al., 2017). Similarly, IVM through imaging windows demonstrated a previously unknown mechanism of intestinal crypt fusion alongside the previously described crypt fission, which may underlie the regulation of the crypt number in the adult mouse (Fig. 1E; Bruens et al., 2017).

This wide range of IVM tools and applications has not only shed new light on normal biology and tissue homeostasis but also had an impact on our current understanding of cancer progression and treatment, which will be discussed in detail below.

Intravital cancer imaging at primary and secondary sites

Several approaches have been taken to label the tumour and its microenvironment using GEMMs, bioluminescence, or untargeted or targeted labelling of cells or their surrounding environment (see Table 1), with the aim of tracking cancer progression, metastasis and treatment (Ilhan-Mutlu et al., 2016; Jung et al., 2017; Osswald et al., 2015; Park et al., 2016b). In this context, IVM can be used to monitor cancer and stromal cells, thereby helping to characterise spatiotemporally dynamic events, such as local cancer invasion and distant metastases, as well as evaluating targets of drug treatment or pharmacodynamics and

Journal of Cell Science (2018) 131, jcs206995. doi:10.1242/jcs.206995

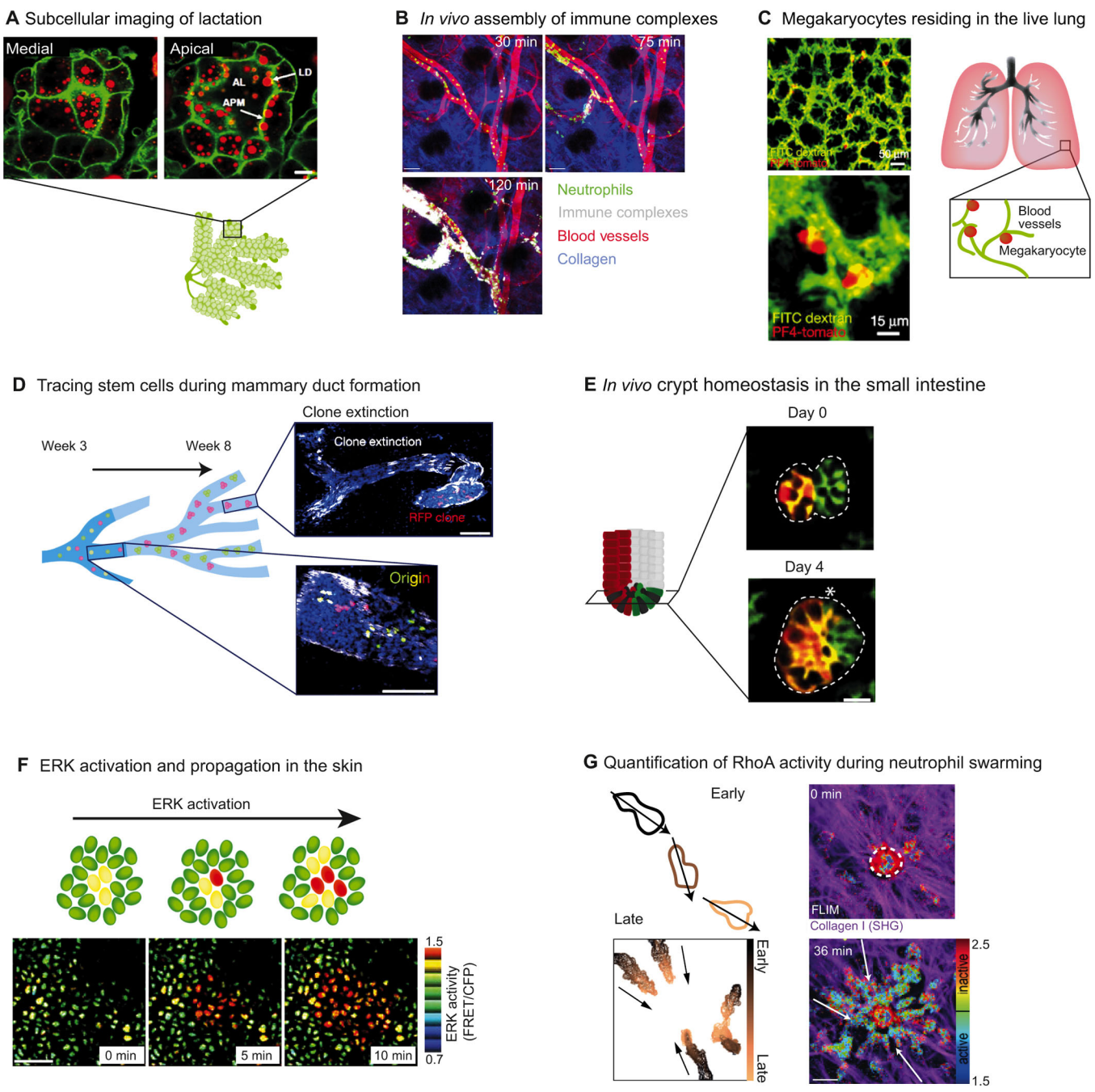

Fig. 1. See next page for legend.

pharmacokinetics (Conway et al., 2014; Dubach et al., 2017; Miller and Weissleder, 2017).

For example, IVM tracking of the interaction of malignant B-cells with their microenvironment in the calvaria was used to delineate the upstream regulators of α4β1 integrin activity in cancer cell adhesion *in vivo*, which could in future be targeted to disrupt interactions between cancer cells and their environment in this hard-to-treat site (Martínez-Moreno et al., 2016). Another study described the bone marrow seeding of leukaemia cells *in vivo* and their transient and promiscuous interactions with their microenvironment (Fig. 2A; Hawkins et al., 2016). Here, IVM revealed a progressive remodelling of the bone marrow microenvironment during disease progression that was confirmed in biopsies from human patients, which emphasises the value of IVM in pre-clinical models to gain insights into disease aetiology (Hawkins et al., 2016).

Similarly, IVM was used to demonstrate heterogeneity in cell motility and the mode of cell migration in melanoma. These intravital findings were combined with transcriptomic analysis to identify gene networks that are differentially expressed between motile and non-motile cells and these may represent potential predictors of cell mobility and invasiveness in patient samples (Manning et al., 2015). IVM tracking also showed that changes in breast tumour cell velocity, in response to the LIM domain kinase (LIMK) inhibitor Pyr1, depended on the morphology of the tumour cell *in vivo* (Prunier et al., 2016), where, upon drug treatment, elongated cells slowed down, whereas round cells sped

Fig. 1. Intravital microscopy imaging in normal tissue. (A) IVM of lipid droplet secretion in the surgically exposed lactating mammary gland of genetically engineered mice expressing cell membrane-localised GFP (mammary epithelial cells, GFP, green; milk lipid droplets, BODIPY, red; scale bar: 10 µm). AL, alveolar lumen; APM, apical plasma membrane; LD, lipid droplet. (B) *In vivo* immune complex formation in the ear after injection of an anti-BSA antibody followed by systemic administration of fluorescently labelled BSA antigen (30, 75 and 120 min after injection). Immune complexes can be taken up and transported into the interstitium by neutrophils (EGFP-expressing neutrophils, green; AF555-labelled immune complexes, white; Evans Blue-labelled vasculature, red; collagen I-derived SHG signal, blue; scale bar: 50 µm). (C) Identification of extravascular megakaryocytes by intravital lung imaging through thoracic windows in *PF4-Cre×Gt(ROSA)26Sortm9(CAG-tdTomato)Hze* mice. (D) Tracking of clonal outgrowth during mammary gland development in *R26-Confetti;R26-CreERT2* lineage tracer mice; here, Confetti expression was induced by tamoxifen-mediated Cre recombination. Over the course of development, subclones of mammary stem cells are randomly segregated, leading to single-coloured clones or clone extinction in ducts that formed late during development (compare existence of multi-coloured clones for week 3 with single-coloured clones or clone extinction during week 8; GFP clone, green; RFP clone, red; scale bars: 100 µm). (E) Intravital tracking of crypt fusion in the small intestine through abdominal imaging windows in *Lgr5$^{EGFP\text{-}ires\text{-}CreERT2}$; LSL-tdTomato* mice; here, low-level recombination of the tdTomato allele was used to label individual crypts with tdTomato (tdTomato, red; EGFP, green; scale bar: 20 µm). Asterisk indicates competing cells. (F) Radial ERK1/2 activation dynamics observed by longitudinal IVM in the basal layer of the ear epidermis of genetically engineered ERK-FRET biosensor mice. ERK1/2 activity was measured using ratiometric FRET imaging of CFP and YFP and is illustrated using a rainbow colour palette. Scale bar: 30 µm. (G) Intravital quantification of RhoA activity in swarming neutrophils using FLIM-FRET imaging in *LysM-Cre; RhoA-FRET* mice, where RhoA-FRET reporter expression in neutrophils is induced via LysM-Cre-mediated recombination. Laser ablation of a resident ear dendritic cell created a local site of tissue damage (white dashed circle) to which the neutrophils migrated (compare 0 min with 36 min; see also illustration on left). Fluorescence lifetime is illustrated using a standard rainbow colour look-up table ranging from 1.5 to 2.5 ns. Scale bar: 50 µm. Images in A adapted from Masedunskas et al. (2017) under https://creativecommons.org/licenses/by-nc-sa/3.0/. Images in B reprinted from Li et al. (2016a), with permission from Elsevier. Images in C and D, adapted from Lefrancais et al. (2017) and Scheele et al. (2017), respectively, with permission from Macmillan Publishers Ltd. Images in E,F,G adapted from Bruens et al. (2017), Hiratsuka et al., (2015), Nobis et al. (2017), respectively, under https://creativecommons.org/licenses/by/4.0/legalcode.

up. This demonstrated a transient response to drug treatment in individual cells depending on cellular morphology and treatment timing, which cannot be observed in fixed tissue samples, but is important to guide future treatment regimens. Similarly, single-cell analysis in pancreatic cancer has also revealed heterogeneity in response to treatment (Erami et al., 2016; Nobis et al., 2017, 2013).

Furthermore, the pharmacodynamics and pharmacokinetics of chemotherapy can often be elucidated using IVM. For example, IVM demonstrated that tumour cells display delayed onset of cell death following treatment with paclitaxel *in vivo* compared with cancer cells examined *in vitro*, highlighting that the tumour microenvironment influences chemotherapeutic efficacy (Orth et al., 2011). Moreover, for detailed characterisation of *in vivo* pharmacokinetics, a fluorescent analogue of the chemotherapeutic drug eribulin was administered and imaged through a window chamber in a mouse model of spatially heterogeneous expression of taxane resistance (Laughney et al., 2014). Here, resistant cells, visualised by the high expression of a fluorescent multi-drug resistance 1 (MDR1) fusion protein, did not accumulate the eribulin analogue, whereas MDR1 inhibition improved its intracellular accumulation. Importantly, such single-cell readouts of drug uptake and efficacy can help to provide real-time insight into the mechanisms of drug efficacy and drug resistance *in vivo* and to establish optimised treatment regimens to overcome the intratumoural heterogeneity in drug response and resistance.

IVM can also provide novel insights into dynamic aspects of the metastatic cascade *in vivo*, such as epithelial-to-mesenchymal transition (EMT), which can often precede and permit cancer metastasis, and mesenchymal-to-epithelial transition (MET), which might allow metastatic cancer cells to colonise secondary sites. Zhao et al. (2016) simultaneously observed *in vivo* EMT alongside changes in cell migration and morphology in the MMTV-PyMT model of invasive and metastatic breast cancer, in which expression of the oncoprotein polyoma middle T antigen (PyMT) under the control of the mouse mammary tumour virus long terminal repeat (MMTV-LTR) drives cancer progression (Lin et al., 2003). Here, IVM can provide insight into single-cell EMT events in their native environment, as well as distinct real-time readouts of drugs targeting the EMT process or cells that have undergone EMT (Zhao et al., 2016). De-regulated expression of the cell–cell junction protein E-cadherin is also often associated with EMT and cell invasiveness (Gregory et al., 2008; Lehmann et al., 2016b). Using a GEMM with fluorescent protein expression from the endogenous E-cadherin locus to monitor changes in E-cadherin expression intravitally, Beerling et al. (2016) demonstrated epithelial–mesenchymal plasticity in breast cancer. They show that mesenchymal cells with low E-cadherin expression have a similar potential as epithelial cells with high E-cadherin expression to give rise to epithelial metastases. This indicates that cancer cells can rapidly switch between epithelial and mesenchymal states *in vivo*, which may support them in adapting to new environments and promoting secondary growth (Fig. 2Bi; Beerling et al., 2016). Therefore, IVM can help to determine the epithelial–mesenchymal status of cancer cells and the optimal timing of drug treatment to most effectively counteract EMT and MET switching during the transit of cancer cells to secondary sites.

Cancer cells can also invade and metastasise in the absence of EMT, retaining and positively utilising E-cadherin expression for locomotion. Indeed, it was recently demonstrated that cancer-associated fibroblasts (CAFs) can support collective cancer cell invasion (Gaggioli et al., 2007; Labernadie et al., 2017; Sanz-Moreno et al., 2011). For example, heterophilic interaction between CAF N-cadherin and cancer cell E-cadherin results in the transduction of mechanical forces that pull cancer cells away from the primary tumour and re-polarise CAFs, resulting in a net collective movement (Fig. 2Bii; Labernadie et al., 2017). Similar heterotypic interactions have been observed in border cell migration in *Drosophila* and other collective movements in development (Cai et al., 2014; Kardash et al., 2010; Wang et al., 2010) and thus may be a process co-opted in cancer to facilitate collective migration (Friedl and Gilmour, 2009; Ilina and Friedl, 2009).

Photoconversion and the use of photoswitching proteins offer another excellent opportunity to follow cell invasion and metastasis. For example, tracking of photoswitched mammary tumour cells showed that, compared with primary tumour cells distant from blood vessels, cells in close proximity to blood vessels migrate extensively within and outside of the primary tumour, and later on, are also detectable at secondary sites (Kedrin et al., 2008). Similarly, genetically engineered murine and patient-derived colon organoids that express known mutational drivers of colorectal cancer progression and metastasis were longitudinally tracked following photoswitching to define the cumulative mutational load required for tumour cell migration and subsequent metastasis (Fumagalli et al., 2017). This study demonstrated that a combined mutational load affecting several signalling pathways allows colorectal cancer

Journal of Cell Science (2018) 131, jcs206995. doi:10.1242/jcs.206995

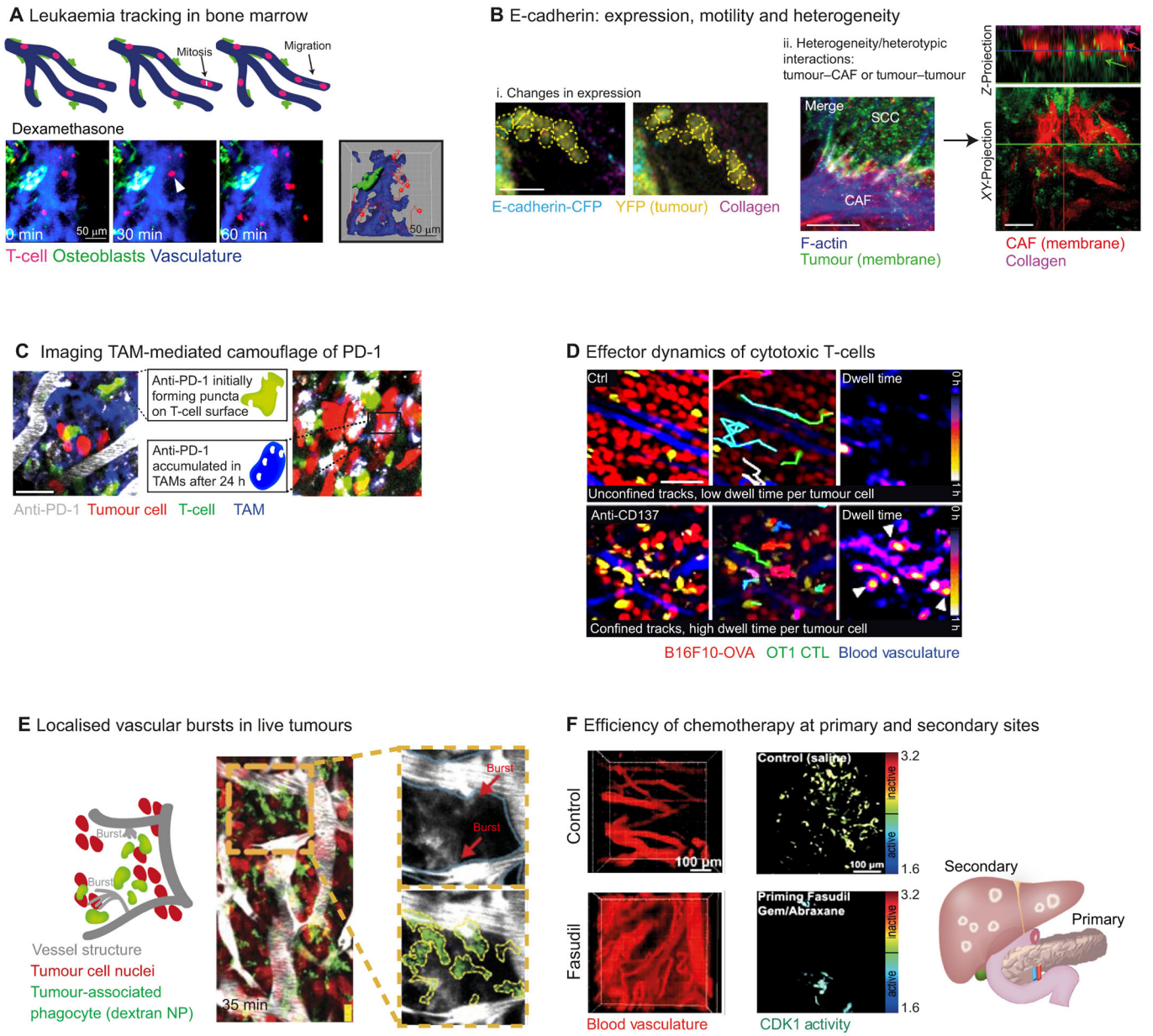

Fig. 2. Intravital microscopy imaging in disease tissue. (A) Intravital tracking of mitosis in leukaemia cells (white arrowhead) and their transient interactions with the calvarium bone microenvironment upon Dexamethasone treatment through surgically inserted imaging windows (Ds-Red-labelled T-cells, red; Col2.3-GFP-labelled osteoblasts, green; Cy5-dextran-labelled vasculature, blue). (B) Cancer cells can modulate their cell–cell junctions for efficient invasion and metastasis.(i) IVM of mobile mammary tumour cells with downregulated expression of the cell–cell junction protein E-cadherin, a feature of epithelial–mesenchymal transition. Scale bar: 25 µm. (ii) Heterotypic interaction between E-cadherin on cancer cells and N-cadherin on cancer-associated fibroblasts (CAFs) can promote cancer cell invasion. Here, IVM demonstrated the close contact between A431 squamous cell carcinoma (SCC) cancer cells (green) and patient-derived CAFs (red), which were co-injected into the mouse ear. Scale bars: 5 µm (left) and 10 µm (right). (C) IVM of tumour-associated macrophages (TAMs) removing cytotoxic T-cell (CTL)-targeted anti-PD1 drug from the cell surface, thereby decreasing immunotherapy performance. Scale bar: 30 µm. (D) Intravital tracking of CTL migration and interaction with cancer cells in dorsal skinfold chambers to optimise immunotherapy performance *in vivo*. By using IVM, the combined adoptive transfer of activated anti-OVA OT1 T-cells and treatment with an anti-CD137 antibody was shown to improve tumour rejection compared with single treatments through the slow down of CTL migration and the prolonging of interactions between CTLs and tumour cells (arrowheads). Scale bar: 50 µm. (E) IVM illustrates dynamic permeability (bursts) in tumour-associated blood vessels upon radiotherapy with phagocyte accumulation at the site of local vascular burst. This could be exploited for improved nanoparticle delivery into the tumour (53BP1-mApple-expressing HT1080 tumour cell nuclei, red; VT680XL-Ferumoxytol-labelled phagocytes, green; Oregon Green dextran-labelled blood vessels and extravasation, white; scale bar: 20 µm). (F) Monitoring improved chemotherapy efficacy using a CDK1-FRET biosensor at secondary sites upon combination with the small-molecule ROCK inhibitor Fasudil, which induces vascular leakage in primary pancreatic tumours (left; QD655 Quantum Dot-labelled blood vessels and leakage, red) and increases Gemcitabine/Abraxane efficacy and cell cycle arrest as visualised by increased CDK1 activity (right). Fluorescence lifetime is illustrated using a standard rainbow colour look-up table ranging from 1.6 to 3.2 ns. Images in A and Bii adapted from Hawkins et al. (2016) and Labernadie et al. (2017), respectively, with permission from Macmillan Publishers Ltd. Images in Bi adapted from Beerling et al. (2016) under https://creativecommons.org/licenses/by-nc-nd/4.0/legalcode. Images in C, E,F adapted from Arlauckas et al. (2017), Miller et al. (2017),Vennin et al. (2017), respectively, with permission from AAAS. Image in D adapted from Weigelin et al. (2015).

Journal of Cell Science (2018) 131, jcs206995. doi:10.1242/jcs.206995

Table 1. Environmental label-free imaging

Imaging technique	Description	Application
Second harmonic generation (SHG)	Two photons simultaneously interact with non-centrosymmetric structures (e.g. collagen, myosin and microtubules) generating a photon with doubled energy and halved wavelength. Only a limited number of molecules provide second harmonic properties for imaging. Provides good optical sectioning without photo-toxicity or photobleaching but requires multiphoton excitation.	Imaging of fibrillar collagen in tissues including muscle, skin and tumours (Brown et al., 2003; Campagnola et al., 2002; Koenig and Riemann, 2003; Kular et al., 2015; Plotnikov et al., 2006; Zipfel et al., 2003) Imaging of fibrillar collagen in human breast tissue in relation to mammographic density (Huo et al., 2015), during cancer cell invasion (Andrlová et al., 2017) or anti-cancer drug targeting of the stromal ECM (Chang et al., 2017; Miller et al., 2015; Vennin et al., 2017)
Third harmonic generation (THG)	Excitation primarily occurs at water–lipid and water–protein interfaces, to provide structural information (e.g. cell morphology and surrounding ECM). Combination with other fluorescent detection modalities to obtain morphological and biochemical information. Like SHG, requires multiphoton excitation.	Imaging cell invasion (Olivier et al., 2010; Rehberg et al., 2010; Tsai et al., 2012; Weigelin et al., 2012) Combination with theranostics (Harpel et al., 2016) Optical biopsies (Chen et al., 2010; Kuzmin et al., 2016; Liao et al., 2013; Tsai et al., 2014)
Optical coherence tomography (OCT)	Cross-sectional, high-resolution tomographic imaging of tissue microstructure by interferometric measurement of backscattered light. Limited resolution compared with other microscopy approaches.	Assessing/identifying tumour margins (Alawi et al., 2013; Nguyen et al., 2009) Cancer diagnosis (Chen et al., 2007; Gora et al., 2013; Karl et al., 2010; Kim et al., 2009) Combined OCT and Raman spectroscopy to detect colon and breast cancers based on signature of lipids, collagen and DNA (Ashok et al., 2013; Patil et al., 2008)
Coherent anti-Stokes Raman scattering (CARS)	Uses vibrational frequency of chemical bonds to generate contrast in lipid bilayers, cell membranes, adipocytes, DNA, myelin sheaths or foam cells of atheroma. Weak signals can be masked by fluctuations of the non-resonant background.	Multi-modal CARS imaging for pathological detection and live imaging of cancer (Evans and Xie, 2008; Evans et al., 2007; Heuke et al., 2013; Lee et al., 2015; Lee and Serrels, 2016; Meyer et al., 2011; Meyer et al., 2013; Xu et al., 2013b) Link metabolic changes to disease (Le et al., 2009, 2007) with ongoing advances in CARS endoscopy (Légaré et al., 2006)
Fluorescence lifetime imaging microscopy (FLIM) of endogenous compounds	Signals from endogenous compounds, such as flavins, retinol, keratin, melanin or elastin can be observed by analysing the spectroscopic properties of the emission using FLIM.	Metabolic mapping via NAD/NADH or FAD imaging (Huck et al., 2016; Kasischke et al., 2011; Malik et al., 2016; Skala et al., 2007; Szulczewski et al., 2016)

cells to grow independently of signals from their microenvironment and so promote metastasis.

IVM therefore serves as a versatile tool to obtain detailed spatiotemporal information of disease progression and to pinpoint those stages of cancer progression that are most vulnerable to drug action *in vivo* for improved pre-clinical characterisation of drug treatment regimens.

IVM of the tumour-associated immune system

In vivo imaging has been used to characterise the dynamic interactions between cancer cells and the tumour-associated immune system, which are known to have a key role in cancer progression, metastasis and treatment. For instance, labelling of tumour-infiltrating immune cells by *in vivo* photoconversion showed that some immune cell types are retained in the primary tumour, whereas others, such as effector T-cells, which play a role in anti-tumour immunity, can readily migrate to draining lymph nodes and even to secondary tumour sites (Torcellan et al., 2017). These findings could be further explored to promote T-cell-mediated anti-tumour immunity at secondary sites. IVM has also been used to monitor the pro-metastatic support that immune cells can confer to cancer cells. Intravital lung imaging through windows showed the formation of neutrophil extracellular traps (NETs), which are an extracellular network of DNA and cytotoxic enzymes released by neutrophils to bind and kill pathogens (Park et al., 2016a). In the absence of infection, breast cancer cells could induce NET formation, thereby stimulating cancer invasiveness and metastasis, which could be inhibited upon administration of DNaseI-containing nanoparticles (Park et al., 2016a). Similarly, IVM of the lung immune response upon metastatic seeding showed that many metastatic pioneer cells, which are released from the primary tumour into the circulation, fragmented upon shear stress within blood vessels (Headley et al., 2016). The resulting microparticles were taken up by immune cells that arrived at the metastatic niche in distinct waves. Using GEMMs, which lack distinct subsets of immune cells, the authors showed that microparticle-containing myeloid cells might promote metastatic seeding, whereas a rare dendritic cell subtype, which also ingested microparticles, was found to have anti-metastatic effects, highlighting the dual nature of the immune response to metastasis (Headley et al., 2016). These observations exploited the transfer of the fluorescent label from cancer cells into the tumour-ingesting immune cells by phagocytosis; many IVM approaches make use of such inherent cellular processes. For example, IVM demonstrated that fluorescently labelled bisphosphonates, which have been shown to possess anti-tumour activity, were taken up by tumour-associated macrophages (TAMs), potentially corrupting their tumour-promoting functions (Junankar et al., 2015). Here IVM identified

the cell types targeted by bisphosphonates in cancer and provided novel insight into the previously uncharacterised anti-cancer activity of these drugs.

IVM has also been used to assess the performance of immunotherapy or blockade of immune checkpoints. For example, treatment of colorectal cancer, lung cancer and melanoma xenograft models with fluorescently labelled anti-PD1 (PD1 is also known as PDCD1) showed that TAMs take up anti-PD1 from the surface of cytotoxic T-cells (CTLs), which is mediated by FCγ receptors (Fig. 2C; Arlauckas et al., 2017). Based on these observations, combination treatments consisting of FCγR inhibition and anti-PD1 antibodies were tested *in vivo*, which improved immunotherapy performance by extending the time anti-PD1 localised to CTLs (Arlauckas et al., 2017). Similarly, longitudinal IVM of interactions between cancer and immune cells revealed the formation of an immunosuppressive 'ring' of T-regulatory cells around the tumour that can inhibit CTL efficacy (Qi et al., 2016). Indeed, breaking this ring of T-regulatory cells by using cyclophosphamide accelerated CTL infiltration into the tumour.

Moreover, IVM of melanoma immunotherapy contributed to a better therapeutic outcome in mice as it demonstrated that treatment with an anti-CD137 agonist antibody improved the anti-tumour effector functions of both endogenous and transplanted CTLs (Weigelin et al., 2015). Here, anti-CD137 agonist antibody treatment resulted in increased intratumoural CTL viability, reduced CTL migration speed, as well as prolonged interaction between CTLs and tumour cells and thus increased killing efficacy upon contact with a tumour cell (Fig. 2D; Weigelin et al., 2015). IVM has also been used to test the efficacy of new anti-cancer immunotherapy agents. For example, treatment with a new T-cell bispecific antibody that directly links T-cells with cancer cells resulted in faster and more persistent migration of freely moving T-cells, an increase in tumour-associated T-cells, and prolonged interactions between T-cells and cancer cells, all of which accelerate tumour cell death (Lehmann et al., 2016a). Taken together, these studies demonstrate the usefulness of IVM in fine-tuning or enhancing anti-cancer therapy.

IVM of the tumour-associated vasculature

Blood vessels serve as carriers for oxygen, nutrients and drugs, but can also allow tumour cells to spread to distant sites in the body. IVM offers an opportunity to establish functional landmarks of tissue and cancer biology in addition to the anatomical landmarks obtained from immunohistochemistry. Indeed, a distinct tumour microenvironment of metastasis (TMEM) has been described that can be detected in both GEMMs of breast cancer and human breast cancer patients (Harney et al., 2015). IVM in MMTV-PyMT mice demonstrated a local loss of vascular junctions at TMEMs followed by cancer cell intravasation, thereby providing novel insights into the mechanisms of cancer metastasis (Harney et al., 2015). Similarly, IVM of pancreatic tumour xenografts demonstrated different mechanisms of vascular permeability with transient openings of the vessel wall, as well as vascular bursts visualised by the leakage of fluorescently labelled nanoparticles into the adjacent tissue; both mechanisms may support drug delivery into the extravascular tissue (Matsumoto et al., 2016). Future investigation may show whether these observations align with previous research on the TMEM in breast cancer (Harney et al., 2015).

Localised vascular leakage has recently gained attention with regard to potential cancer treatment. IVM of tumour-associated blood vessels, TAMs and fluorescently labelled or therapeutic nanoparticles revealed that radiotherapy increased TAM density and resulted in enlarged and permeabilised blood vessels with an increase in vascular bursts followed by nanoparticle flux into the tumour tissue (Fig. 2E; Miller et al., 2017). Interestingly, TAM accumulation correlated with and was required for vascular bursts following irradiation, and the combination of radiotherapy and therapeutic nanoparticles reduced tumour growth in a TAM-dependent manner (Miller et al., 2017).

However, the induction of localised vascular bursts and extravascular leakage at breast cancer TMEMs has also been observed upon neoadjuvant chemotherapy (Karagiannis et al., 2017). Chemotherapy using paclitaxel enhanced TMEM assembly through an increased infiltration of macrophages and thereby promoted metastasis despite a reduced growth of the primary tumour, whereas inhibition of TMEM activity reduced these pro-metastatic effects. Another approach to exploit vascular permeability for improved nanoparticle delivery is the localised depletion of tumour-associated platelets, which have been shown to preserve the integrity of tumour-associated blood vessels (Li et al., 2017).

Future detailed intravital monitoring of the tumour microenvironment in the presence or absence of therapy is likely to provide additional insights into the role of localised vessel permeability with the aim to balance localised vascular permeability to improve drug delivery without opening the floodgate to metastasis.

Assessing effects of exosomes using IVM

IVM can be used to better understand cancer cell–cell communication at a distance. Extracellular vesicles (EVs) or exosomes can carry nucleic acids, proteins or lipids to transfer information between cells (reviewed in detail in Becker et al., 2016; Raposo and Stoorvogel, 2013). For example, invasive and metastatic cancer cells can secrete EVs or exosomes that contain pro-invasive and pro-metastatic 'signals' (Singh et al., 2016; Yokoi et al., 2017; Zomer et al., 2015). Recently, Zomer et al. (2015) used Cre-recombinase-carrying exosomes that induce a switch in fluorescent protein expression upon uptake to identify EV-recipient cells *in vivo*. This showed that EVs derived from malignant cancer cells can enhance the metastatic potential of less-malignant cells, revealing the global challenge we face when treating primary and secondary tumour burden. Similarly, IVM in a glioma mouse model provided novel insight into cancer–stroma communication by demonstrating the uptake of glioma-derived EVs by the stromal microglia and other immune cells *in vivo* (van der Vos et al., 2016). Exosomes have also been shown to promote fast and directional tumour cell migration. Autocrine exosome communication can support and stabilise cell–substrate adhesion and increase the persistence of migration directionality (Sung et al., 2015). Furthermore, exosomes have been shown to be transferred to distant sites, such as liver (Costa-Silva et al., 2015) or lung (Liu et al., 2016), where they manipulate resident host cells, preparing a pre-metastatic niche for efficient metastasis (Hoshino et al., 2015; Peinado et al., 2017).

A number of recent studies investigated the potential of exosomes to deliver anti-cancer cargo into the tumour. For example, application of tumour-targeting exosomes engineered to carry shRNA or siRNA against $Kras^{G12D}$, a common driver mutation in pancreatic cancer, as well as in human pancreatic cancer patients, resulted in improved survival and reduced metastasis (Kamerkar et al., 2017). With refined labelling techniques for EVs and exosomes, further studies may inform us how best to treat primary

Journal of Cell Science (2018) 131, jcs206995. doi:10.1242/jcs.206995

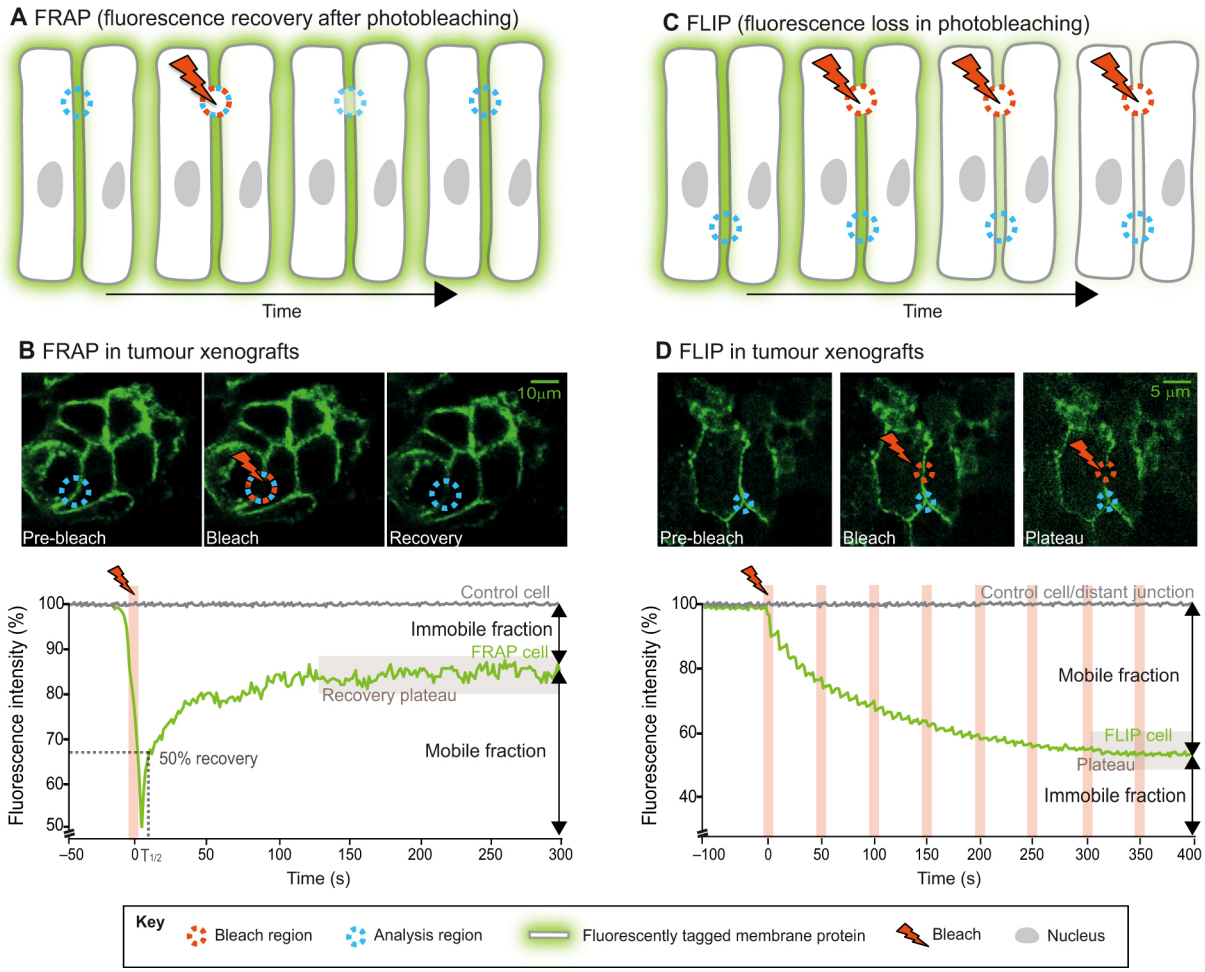

Fig. 3. Subcellular photobleaching in tumours. (A) During fluorescence recovery after photobleaching (FRAP), a small region of interest is bleached (red dashed circle) and fluorescence recovery into the bleached region is monitored (blue dashed circle). (B) Intravital FRAP imaging of E-cadherin–GFP after skin flap surgery in pancreatic tumour xenografts to quantify E-cadherin mobilisation in pancreatic tumour cell–cell junctions (cell–cell junction protein E-cadherin-GFP, green). Fluorescence intensity is plotted over time to determine the half-time of recovery ($T_{½}$, graph, dashed line) and the mobile and immobile fractions of the fluorescently tagged protein. (C) During fluorescence loss in photobleaching (FLIP), the loss of fluorescence intensity upon photobleaching is monitored in an adjacent region. (D) FLIP imaging can complement results obtained from FRAP experiments, as was recently shown in pancreatic tumour xenografts characterizing E-cadherin mobilization. Using continuous photobleaching, it is possible to quantify the mobile and immobile fractions of the fluorescently tagged protein based on the obtained FLIP graph. All cell images adapted from Erami et al. (2016) under https://creativecommons.org/licenses/by/4.0/legalcode.

versus metastatic disease (Steeg, 2016) and prevent communication with other cancer cells and distant sites (Peinado et al., 2017). Future IVM studies may thus provide further insight into the multifaceted role of EVs in disease progression.

Subcellular intravital photobleaching

Subcellular IVM approaches (Box 1) can be used to probe dynamic subcellular processes, such as protein dynamics, protein–protein interactions or protein activity, making these techniques attractive to assess the molecular basis of cancer progression and treatment at a level beyond the single-cell level discussed above. For example, photobleaching techniques, such as fluorescence recovery after photobleaching (FRAP; Fig. 3A) and fluorescence loss in photobleaching (FLIP, Fig. 3C), can be used to characterise the mobility of fluorescently tagged proteins or fluorescent agents (see Fig. 3 and Box 1 for further details).

The use of photobleaching IVM has provided many insights into the molecular dynamics of key biological processes in intact tissues. For example, Machado and Mitchell (2011) used a dorsal skinfold chamber model to track blood vessel ingrowth into a wound site upon heat injury. Using intravital FRAP imaging of FITC-dextran during re-vascularisation they were able to distinguish between vessels of different maturity based on their fluorescence recovery profiles and half-times of recovery. Elegant studies in human tumour xenografts have used FRAP to show how ECM abundance and cellular geometry affects interstitial mobility and diffusion of macromolecules and propose the reduction of ECM content as a potential measure to overcome chemoresistance (Netti et al., 2000; Pluen et al., 2001).

Other IVM studies suggest that increased mobilisation of E-cadherin in cell–cell junctions may be a feature of migrating cells (Canel et al., 2010; Serrels et al., 2009). Recently, an E-cadherin–GFP GEMM was combined with subcellular FRAP and FLIP imaging to provide further insight into *in situ* E-cadherin dynamics in a tissue-specific microenvironmental context (Fig. 3B,D; Erami et al., 2016). FRAP and FLIP analyses revealed that E-cadherin is mobilised in invasive pancreatic cancers that are driven by mutations in both *Kras* and *Tp53* compared with a non-invasive pancreatic cancer model driven by *Kras* mutation and loss of *Tp53*. Because *KRAS* and *TP53* are commonly mutated in the human

Journal of Cell Science (2018) 131, jcs206995. doi:10.1242/jcs.206995

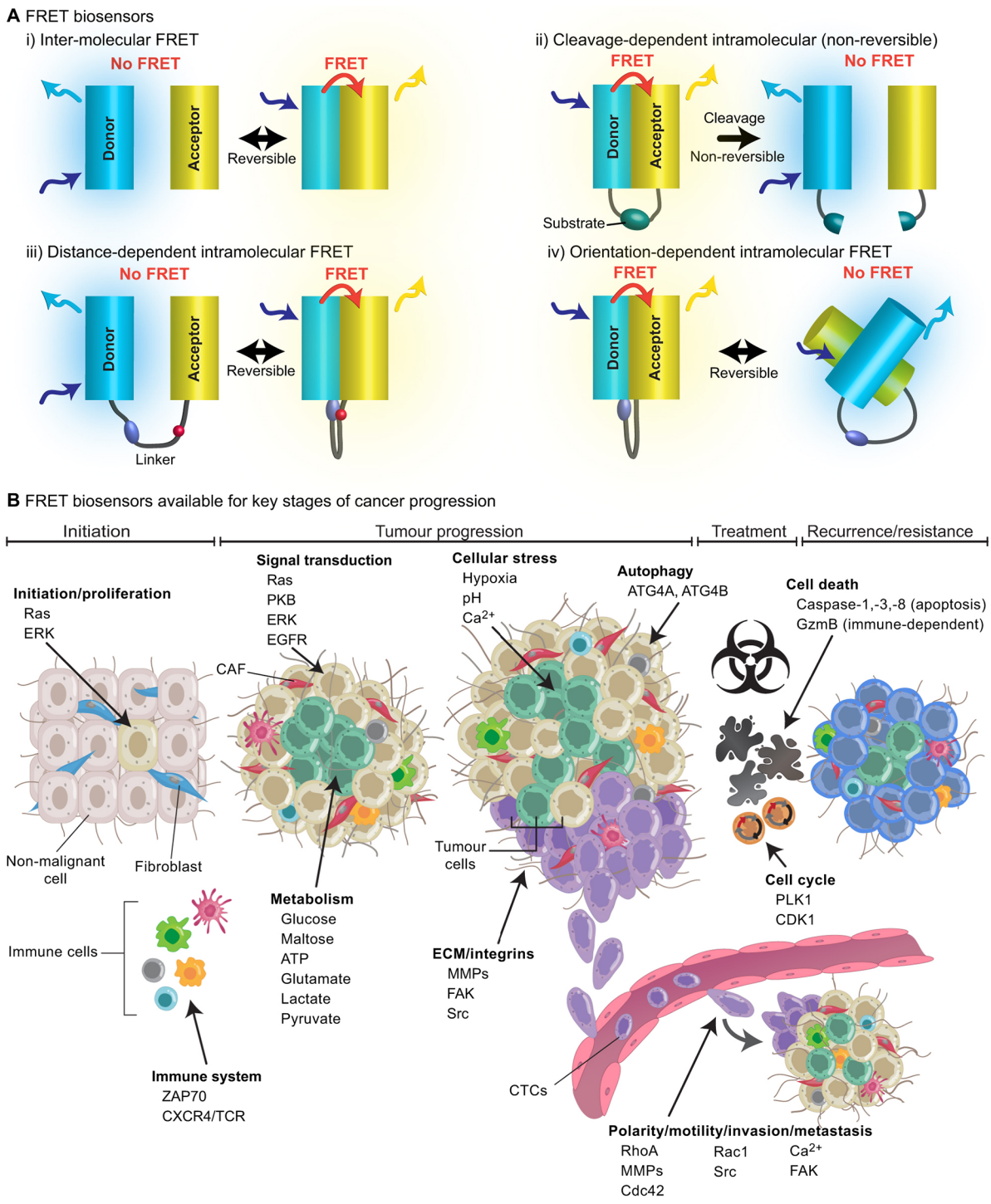

Fig. 4. Förster resonance energy transfer (FRET) biosensors used to characterise cancer aetiology. (A) Examples of different biosensor designs: (i) intermolecular FRET between unlinked fluorophores; (ii) cleavage-dependent FRET, where cleavage of the linker peptide results in an irreversible conformational change; (iii) distance-dependent intramolecular FRET where post-translational modification of the linker peptide affects the distance between donor and acceptor fluorophore; (iv) orientation-dependent FRET, where post-translational modification of the linker peptide affects the alignment of donor and acceptor fluorophore. (B) Different biosensors have been designed to quantify the molecular activity across a range of biological processes, which are also important in disease aetiology, such as cancer, including cell proliferation, cell cycle progression, cell survival, cell polarity, cell migration, cell–ECM interaction, signal transduction, cell metabolism, cellular stress or autophagy. The targeted expression of FRET biosensors makes it possible to precisely read out molecular activity in cancer cells, as well as in stromal components, such as fibroblasts, endothelial cells or immune cells, which are all known to impact cancer progression and response to treatment. ATG4, autophagy-related 4; CAF, cancer-associated fibroblast; Cdc42, cell division cycle 42; CDK1, cyclin-dependent kinase 1; CTC, circulating tumour cell; CXCR4, C-X-C motif chemokine receptor 4; ECM, extracellular matrix; ERK, extracellular signal-regulated kinases 1 and 2; FAK, focal adhesion kinase; GzmB, Granzyme B; MMP, matrix metalloproteinase; PKB, protein kinase B; PLK1, polo-like kinase 1; Rac1, Ras-related C3 botulinum toxin substrate 1; RhoA, Ras homology gene family member A; TCR, T-cell receptor; ZAP70, zeta chain of T-cell receptor-associated protein kinase 70. This is a non-exhaustive list of FRET biosensors and greater detail can be found in Conway et al. (2014, 2017) and Newman et al. (2011).

disease (Biankin et al., 2012), live FRAP and FLIP imaging could be used to visualise the subtle but important dissolution of tumour cell–cell junctions during early stages of pancreatic tumour mobilisation *in vivo*. Such an approach was subsequently used to assess anti-invasive drug targeting *in vivo* to target early invasion or pre-EMT events.

Subcellular intravital FRET imaging

Genetically expressed Förster resonance energy transfer (FRET) biosensors have been used to visualise the subcellular activation status of selected proteins or signalling pathways in an intravital context (see Fig. 4 and Box 1 for further details). For instance, intravital FRET imaging of cell cycle arrest using a CDK1-FRET biosensor (Fig. 4B) was used to optimise chemotherapy performance in murine and patient-derived models of pancreatic cancer by whole-body priming with the ROCK inhibitor Fasudil (Fig. 2F; Vennin et al., 2017). By imaging the biosensor alongside the ECM architecture and vessel leakiness, a transient manipulation of the stromal ECM, rather than chronic treatment, was shown to be effective in improving chemotherapy efficacy. Similarly, Hirata et al. (2015) used intravital FRET imaging of an ERK-FRET biosensor (Fig. 4B) to demonstrate that the BRAF inhibitor PLX4720 activates melanoma-associated fibroblasts, which drive ECM production, remodelling and stiffening to protect melanoma cells against BRAF inhibition. Here, the combination of PLX4720 with FAK (also known as PTK2) inhibition, which targets the integrin-β1–FAK–Src signalling axis restored the vulnerability of melanoma cells to BRAF inhibition. Simultaneous fluorescence and FRET imaging was used in a different study to assess both cell cycle progression through photoswitching of H2B-Dendra and the onset of apoptosis with a Caspase-3 FRET biosensor (Fig. 4B) in the same cell upon docetaxel treatment (Janssen et al., 2013). Here, differences in drug response between *in vitro* and *in vivo* settings were observed: *in vitro*, docetaxel induces cell death via mitotic perturbation, whereas *in vivo*, docetaxel induces apoptosis independently of mitotic defects, emphasising the need to assess drug targeting *in vivo*. Validated FRET biosensors have been discussed in detail previously (Conway et al., 2014, 2017; Newman et al., 2011).

Mice can also be genetically engineered to express FRET biosensors to assess protein activity *in situ*. For instance, novel FRET biosensor mice for Caspase-1 and Caspase-3 activity (Fig. 4B) were used to image single-cell apoptotic events (Liu et al., 2014; Yamaguchi et al., 2011). Similarly, Kamioka and colleagues recently reported the generation of Eisuke-FRET and PKAchu-FRET mice to quantify the dynamics of two major signal transducers, ERK1/2 (collectively known as ERK and also known as MAPK3 and MAPK1) and PKA, respectively (Fig. 4B; Kamioka et al., 2012). Intracellular signalling via ERK and PKA during tissue homeostasis, wound healing, inflammation and upon drug targeting could be correlated with the live cellular phenotype observed (Kamioka et al., 2012; Mizuno et al., 2014, 2016; Sano et al., 2016). Furthermore, these FRET biosensor mice allowed the spatiotemporal assessment of cell signalling and pharmacodynamics in live tissue, such as the temporal propagation of ERK signalling in the epidermis (Fig. 1F; Hiratsuka et al., 2015) or the spatial heterogeneity in ERK signalling in breast tumours (Kumagai et al., 2015).

FRET biosensor mice represent a valuable tool to study the activity of difficult-to-assess signalling molecules such as rapidly switching small GTPases, which are active in the GTP-loaded state and inactive in the GDP-loaded state. This rapid change and the lability of active GTPases *ex vivo* make it difficult to quantify their activation via traditional biochemical approaches (Samuel et al., 2011). Recently, the generation of FRET biosensor mice for two prototypical members of the Rho family of small GTPases, Rac1 and RhoA, has been reported (Fig. 4B; Johnsson et al., 2014; Nobis et al., 2017). These FRET biosensor mice were used to showcase the dynamic regulation of small GTPase activity *in vivo*; live-imaging demonstrated oscillations in activity during directional neutrophil migration (Fig. 1G), regulation of activity during cyclic mammary gestation, co-option of small GTPase activity during breast and pancreatic cancer progression or valuable pharmaco-dynamic readouts during drug intervention.

Simultaneous imaging of several FRET biosensors for multiplexed readout of several signalling pathways has also been achieved through the excitation of several donor fluorophores using the same wavelength (Demeautis et al., 2017; Laviv et al., 2016). For example, Demeautis et al. (2017) reported dual FRET quantification of ERK and PKA FRET biosensors in the same cell to dissect the hierarchies, crosstalk and combinatorial inputs of intracellular signalling pathways. Similarly, a pair of new red fluorescent proteins was imaged in combination with an EGFP-Venus FRET biosensor *in vivo*, where CyRFP could be excited simultaneously with EGFP without an overlap of their emission spectra (Laviv et al., 2016), demonstrating that the simultaneous assessment of multiple protein activities is feasible.

Future applications and combined imaging modes

As discussed above, intravital FRAP and FRET imaging can provide pivotal insights into the subcellular regulation of protein dynamics and activity. However, these approaches are limited by the optical restrictions of confocal laser scanning and multiphoton microscopy, including magnification, resolution or imaging depth. New multimodal imaging approaches whereby IVM is combined with electron microscopy, such as intravital correlative light and electron microscopy (CLEM) can help to reveal ultrastructural details of cells and ECM. The coupling of IVM in live tissue and electron microscopy in fixed tissue imposes several challenges on the user, including tissue fixation or retrieving the IVM region of interest (ROI) in the EM sample (discussed in more detail in de Boer et al., 2015; Follain et al., 2017; Karreman et al., 2016a). For example, near-infrared branding (NIRB) was used to permanently label intravital ROIs and to precisely localise them in the EM sample. This technology was used to reveal ultrastructural details of the microenvironment of rare cell biological events, such as cancer cell extravasation into the brain, which without prior IVM localisation may be challenging to find in a fixed sample (Karreman et al., 2016b).

Another approach to retrieve IVM ROIs *ex vivo* is cryosection labelling and intravital microscopy (CLIM), where intravitally imaged tissue is locally and permanently labelled by phototattooing of collagen fibres prior to fixation and embedding. This allows the user to identify and further analyse IVM ROIs *ex vivo*, as exemplified by the immunohistochemical characterisation of the microenvironments of migratory and non-migratory breast cancer cells (Ritsma et al., 2013a). Recent developments in intravital focusing of cells (Galanzha et al., 2016) or in matrix-assisted laser desorption/ionisation (MALDI) imaging (Grey et al., 2009) may open further avenues for combining IVM data with either *in vivo* flow cytometry applications or spatial proteomics.

Previously inaccessible tissues may be imaged using microendoscopic devices for IVM in awake animals; this recently allowed the simultaneous characterisation of behaviour and the quantification of Ca^{2+} dynamics (Ghosh et al., 2011) or of ERK and PKA signalling activity (Goto et al., 2015). Furthermore, new

optical clearing techniques for large mammalian systems, such as Clarity, Scale, CUBIC (clear, unobstructed brain/body imaging cocktails and computational analysis), 3DISCO (3-dimensional imaging of solvent-cleared organs), SeeDB (see deep brain), ISDoT (*in situ* decellularization of tissues) or PACT (photoacoustic computed tomography), have improved the imaging resolution at depth by removing the cellular components of tissues that cause its opacity (Chung and Deisseroth, 2013; Fischer et al., 2017; Mayorca-Guiliani et al., 2017; Richardson and Lichtman, 2015; Tainaka et al., 2014; Tomer et al., 2014; Yu et al., 2017). Future combination of intravital studies with post-intravital optical clearing and subsequent high-resolution imaging, similar to CLEM, may provide new insight into disease aetiology and treatment.

IVM techniques are also used in targeted nanotherapy and phototherapy. For example, Chen et al. (2017) synthetised a near-infrared fluorescent probe that is cleaved by cathepsin B, which is highly expressed in tumour cells, and can subsequently be excited with near-infrared light to generate a cytotoxic agent. The authors tested their concept *in vivo* in subcutaneous tumours and showed that their photodynamic therapeutics approach prevented tumour growth without affecting normal tissues. Similar applications have recently been described to specifically induce the generation of cytotoxic singlet oxygen in cancer cells (Huang et al., 2016b), for the targeted labelling of tumour cells (Yan et al., 2016) or for the improved delivery and uptake of drug-carrying nanovesicles (Huang et al., 2016a), including the use of immune cells for the delivery of nanoparticles into the tumour (Chu et al., 2017).

Intravital multiphoton imaging can be used to detect endogenous autofluorescent compounds, such as ECM or metabolites, without introducing any exogenous labels or genetic modifications (Table 1). Here, label-free fluorescence lifetime imaging microscopy (FLIM, see Box 1 for further details) readily lends itself to applications in humans. For instance, FLIM has been demonstrated in human lung and skin samples to delineate the border of cancer lesions (Galletly et al., 2008; Wang et al., 2017), as well as in capillaries of the fingernail bed and of the forearm *in vivo* (Shirshin et al., 2017) or in the tongue of human volunteers (Cheng et al., 2014), which could also be adapted for the monitoring of oral cancers in humans. In a recent clinical trial, intravital tomography combined with FLIM of metabolites (see Table 1 and Box 1) demonstrated differences in mitochondrial density between healthy and inflamed skin and that an increase of free NADH in mitochondria correlated with the severity of inflammation (Huck et al., 2016). Thus, this approach could potentially be applied for the early identification of low-inflammation events and thus earlier intervention.

IVM has already been employed in human melanoma patients to image intravenously infused fluorescein to assess tumour vasculature and vascular patency (Fisher et al., 2016). By imaging tumour vessels through an incision into the skin, blood vessels were found to have an enlarged diameter in the *in vivo* setting compared with previous findings from fixed tumour tissues, further emphasising the importance of imaging cells and tissues *in vivo* in their native environment. Future developments in IVM setups such as these are likely to provide opportunities for IVM in the clinical setting.

Challenges and bottlenecks in IVM

IVM imposes a unique set of challenges from a technical perspective, in that users must deal with sample motion, tissue autofluorescence and a complex microenvironment. Another common challenge faced is the large volume of data, as is the case with genomics and proteomics. Here, we briefly discuss recent developments that may help overcome some of these challenges.

Image stabilisation

Currently, there are few commercial packages available that reliably correct for motion artefacts, hence most researchers rely on custom-written software packages. For stable IVM, the animal can be immobilised by using physical restraints or applying negative pressure to reduce tissue motion (Cao et al., 2012; Edelstein et al., 2014; Lee et al., 2012). Residual sample motion due to respiratory or cardiovascular movements can be overcome by synchronising image acquisition with physiological measurements, for example heartbeat (Aguirre et al., 2014; Vinegoni et al., 2015) or respiration (Lee et al., 2012). Image-based stabilisation can also be used to correct for lateral sample motion in post-processing (Fiole et al., 2014; Lee et al., 2014; Soulet et al., 2013; Vercauteren et al., 2006; Vinegoni et al., 2014). Motion of cell–cell junctions during intravital FRAP and FLIP has also been successfully compensated for using optical flow-based techniques (Erami et al., 2016). Axial sample motion in and out of the focal plane cannot be corrected post-imaging. In this case, it may be possible to use real-time correction approaches, where an optical coherence tomography (OCT)-based tracking system was used to adjust the position of the objective in real-time (Sherlock et al., 2015, 2017).

Correcting for sample aberrations

In IVM, penetration depth is often limited by aberration caused by the sample itself, which may be compensated for by using adaptive optics, for instance using a correction collar (Muriello and Dunn, 2008), a deformable membrane mirror (Caroline Müllenbroich et al., 2014) or segmented pupil illumination (Ji et al., 2012; Wang et al., 2014), which can correct for sample aberrations by increasing signal at depth. Alternatively, image-based metrics can be used to estimate the sample aberrations (Burke et al., 2015; Débarre et al., 2009; Song et al., 2010).

Improving acquisition speed

IVM imaging of dynamic and fast events, such as blood flow or mobile immune cells, can be accomplished using resonant scanners, which allow imaging speeds up to 30 frames per second (Kirkpatrick et al., 2012; Matsumoto et al., 2010; Nguyen et al., 2001) or multibeam imaging, which can also reduce photodamage by spreading the excitation power over a number of focal spots (Niesner et al., 2007; Rinnenthal et al., 2013; Shimozawa et al., 2013).

Customisation of imaging setup

Many IVM setups have been customised to adapt to the numerous applications and imaging modalities of IVM, which can easily be adapted and expanded on. Alternatively, they can be assembled from individual software components that control distinct devices, such as stage or scanner, to enable precise control over image acquisition parameters, including HelioScanner (Langer et al., 2013), Micro-Manager (Edelstein et al., 2014) or ScanImage (Pologruto et al., 2003).

Image analysis and quantification

The diverse range of imaging environments for IVM means that custom analysis workflows tend to be developed for each project and few widely used general purpose tools exist. Workflows built with open source packages include ImageJ/Fiji (Schindelin et al., 2012), Icy (de Chaumont et al., 2012), Cellprofiler (Carpenter et al., 2006) or CellCognition (Held et al., 2010), and can complement the

use of commercial tools, e.g. Imaris (Bitplane), Amira (FEI), MetaMorph (Molecular Devices), or Volocity (PerkinElmer). FRAP and FLIP data require quantitative analysis of small subcellular regions over long time periods and, as such, are highly sensitive to sample motion. The image stabilisation software discussed above can be applied directly to photo-bleaching data before analysis with conventional analysis tools (Kraft et al., 2014; Rapsomaniki et al., 2012; Schindelin et al., 2012). Intravital FLIM-FRET with a significant contribution from tissue autofluorescence can be analysed with FLIMfit (Conway et al., 2017; Warren et al., 2013) or phasor-based approaches can be used to separate the contributions from the FRET biosensor and tissue fluorescence (Digman et al., 2008).

Cell tracking and their microenvironment

A wide variety of tools to analyse and model cell migration *in vitro* and *in vivo* have been developed for analysis of cell migration (Alexander et al., 2008; Masuzzo et al., 2016), clonal cell development (Coffey et al., 2013) or for the automated 3D tracking of cells or nuclei (Keller et al., 2008; Li et al., 2007). For example, a study used a multiparametric classification approach to automatically identify tumour cell phenotype and to relate the features they identified to their microenvironmental context (Gligorijevic et al., 2014). Machine learning approaches have also been used to automate longitudinal cell cycle profiling using the fluorescence probe FUCCI (Chittajallu et al., 2015) or to identify haematopoietic stem cells in a heterogenous environment (Khorshed et al., 2015). Other software tools have been developed for the characterisation of cell movement in relation to complex microenvironmental cues, such as collagen orientation (Mayorca-Guiliani et al., 2017; Rezakhaniha et al., 2012), grey-level co-occurrence matrix analysis (GLCM; Cicchi et al., 2010) or gap analysis (Acton et al., 2014).

Big data

Here, guidelines for standardised image acquisition, annotation, storage, analysis and publication may allow for a better comparison between published works and lead to the generation of comprehensive atlases of single-cell and subcellular events. Several open source projects aim to provide a platform for storing, annotating and managing large datasets, such as OMERO (Allan et al., 2012), Bisque (Kvilekval et al., 2010) and Cytomine (Marée et al., 2016). Other projects such as the Image Data Resource (IDR) aim to facilitate the reuse and reanalysis of previously published data by integrating the analysis of multiple, disparate image studies (Williams et al., 2017). This common use and publication of IVM datasets may also maximise the overall scientific output by facilitating the analysis and extraction of information not assessed by the primary study, similarly to that of protein and gene lists derived from large 'omics datasets.

Concluding remarks

In conclusion, we have come a long way in this field from improving fluorophores, imaging components and key tools. The future of IVM as a stand-alone technique or in combination with other research areas, including molecular or cellular 'omics approaches, will help to encourage the use of IVM as part of a standard approach to study disease progression. Importantly, using IVM, will allow us to observe disease in a high-fidelity, functional and more physiological setting which is of the utmost importance if we are to fully understand disease progression and how best to target it.

Acknowledgements

The authors would like to thank Dr Aurélie Cazet, Dr Claire Vennin, James Conway and Daniel Reed for critical reading of the manuscript and apologise to our colleagues for not being able to cite all individual references due to space limitations.

Competing interests

The authors declare no competing or financial interests.

Funding

Work in the authors' lab is supported by the National Health and Medical Research Council (NHMRC; project and fellowship funding), NBCF, Cancer Institute NSW, the Australian Research Council, a Len Ainsworth Pancreatic Cancer Fellowship, Cancer Council NSW, St Vincent's Clinic Foundation and Tour de Cure. This project was made possible by an Avner Pancreatic Cancer Foundation Grant.

References

Abbaci, M., Barberi-Heyob, M., Stines, J.-R., Blondel, W., Dumas, D., Guillemin, F. and Didelon, J. (2007). Gap junctional intercellular communication capacity by gap-FRAP technique: a comparative study. *Biotechnol. J.* **2**, 50-61.

Acton, S. E., Farrugia, A. J., Astarita, J. L., Mourão-Sá, D., Jenkins, R. P., Nye, E., Hooper, S., Van Blijswijk, J., Rogers, N. C., Snelgrove, K. J. et al. (2014). Dendritic cells control fibroblastic reticular network tension and lymph node expansion. *Nature* **514**, 498-502.

Aguirre, A. D., Vinegoni, C., Sebas, M. and Weissleder, R. (2014). Intravital imaging of cardiac function at the single-cell level. *Proc. Natl. Acad. Sci. USA* **111**, 11257-11262.

Alawi, S. A., Kuck, M., Wahrlich, C., Batz, S., Mckenzie, G., Fluhr, J. W., Lademann, J. and Ulrich, M. (2013). Optical coherence tomography for presurgical margin assessment of non-melanoma skin cancer - a practical approach. *Exp. Dermatol.* **22**, 547-551.

Alexander, S., Koehl, G. E., Hirschberg, M., Geissler, E. K. and Friedl, P. (2008). Dynamic imaging of cancer growth and invasion: a modified skin-fold chamber model. *Histochem. Cell Biol.* **130**, 1147-1154.

Allan, C., Burel, J.-M., Moore, J., Blackburn, C., Linkert, M., Loynton, S., Macdonald, D., Moore, W. J., Neves, C., Patterson, A. et al. (2012). OMERO: flexible, model-driven data management for experimental biology. *Nat. Methods* **9**, 245-253.

Andrlová, H., Mastroianni, J., Madl, J., Kern, J. S., Melchinger, W., Dierbach, H., Wernet, F., Follo, M., Technau-Hafsi, K., Has, C. et al. (2017). Biglycan expression in the melanoma microenvironment promotes invasiveness via increased tissue stiffness inducing integrin-beta1 expression. *Oncotarget* **8**, 42901-42916.

Arlauckas, S. P., Garris, C. S., Kohler, R. H., Kitaoka, M., Cuccarese, M. F., Yang, K. S., Miller, M. A., Carlson, J. C., Freeman, G. J., Anthony, R. M. et al. (2017). In vivo imaging reveals a tumor-associated macrophage-mediated resistance pathway in anti-PD-1 therapy. *Sci. Transl. Med.* **9**, eaal3604.

Ashok, P. C., Praveen, B. B., Bellini, N., Riches, A., Dholakia, K. and Herrington, C. S. (2013). Multi-modal approach using Raman spectroscopy and optical coherence tomography for the discrimination of colonic adenocarcinoma from normal colon. *Biomed. Optics Express* **4**, 2179-2186.

Bartholomäus, I., Kawakami, N., Odoardi, F., Schläger, C., Miljkovic, D., Ellwart, J. W., Klinkert, W. E. F., Flügel-Koch, C., Issekutz, T. B., Wekerle, H. et al. (2009). Effector T cell interactions with meningeal vascular structures in nascent autoimmune CNS lesions. *Nature* **462**, 94-98.

Becker, A., Thakur, B. K., Weiss, J. M., Kim, H. S., Peinado, H. and Lyden, D. (2016). Extracellular vesicles in cancer: cell-to-cell mediators of metastasis. *Cancer Cell* **30**, 836-848.

Beerling, E., Seinstra, D., de Wit, E., Kester, L., van der Velden, D., Maynard, C., Schäfer, R., van Diest, P., Voest, E., van Oudenaarden, A. et al. (2016). Plasticity between epithelial and mesenchymal states unlinks EMT from metastasis-enhancing stem cell capacity. *Cell Rep.* **14**, 2281-2288.

Biankin, A. V., Waddell, N., Kassahn, K. S., Gingras, M.-C., Muthuswamy, L. B., Johns, A. L., Miller, D. K., Wilson, P. J., Patch, A.-M., Wu, J. et al. (2012). Pancreatic cancer genomes reveal aberrations in axon guidance pathway genes. *Nature* **491**, 399-405.

Bixel, M. G., Kusumbe, A. P., Ramasamy, S. K., Sivaraj, K. K., Butz, S., Vestweber, D. and Adams, R. H. (2017). Flow dynamics and HSPC homing in bone marrow microvessels. *Cell Rep.* **18**, 1804-1816.

Bochner, F., Fellus-Alyagor, L., Kalchenko, V., Shinar, S. and Neeman, M. (2015). A novel intravital imaging window for longitudinal microscopy of the mouse ovary. *Sci. Rep.* **5**, 12446.

Bolognesi, A., Sliwa-Gonzalez, A., Prasad, R. and Barral, Y. (2016). Fluorescence recovery after photo-bleaching (FRAP) and fluorescence loss in photo-bleaching (FLIP) experiments to study protein dynamics during budding yeast cell division. *Methods Mol. Biol.* **1369**, 25-44.

Bremer, D., Pache, F., Günther, R., Hornow, J., Andresen, V., Leben, R., Mothes, R., Zimmermann, H., Brandt, A. U., Paul, F. et al. (2016). Longitudinal intravital imaging of the retina reveals long-term dynamics of immune infiltration and its

effects on the glial network in experimental autoimmune uveoretinitis, without evident signs of neuronal dysfunction in the ganglion cell layer. *Front. Immunol.* **7**, 642.

Brown, E., Mckee, T., Ditomaso, E., Pluen, A., Seed, B., Boucher, Y. and Jain, R. K. (2003). Dynamic imaging of collagen and its modulation in tumors in vivo using second-harmonic generation. *Nat. Med.* **9**, 796-800.

Bruens, L., Ellenbroek, S. I. J., Van Rheenen, J. and Snippert, H. J. (2017). In vivo imaging reveals existence of crypt fission and fusion in adult mouse intestine. *Gastroenterology* **153**, 674-677.

Burke, D., Patton, B., Huang, F., Bewersdorf, J. and Booth, M. J. (2015). Adaptive optics correction of specimen-induced aberrations in single-molecule switching microscopy. *Optica* **2**, 177-185.

Cai, D., Chen, S.-C., Prasad, M., He, L., Wang, X., Choesmel-Cadamuro, V., Sawyer, J. K., Danuser, G. and Montell, D. J. (2014). Mechanical feedback through E-cadherin promotes direction sensing during collective cell migration. *Cell* **157**, 1146-1159.

Campagnola, P. J., Millard, A. C., Terasaki, M., Hoppe, P. E., Malone, C. J. and Mohler, W. A. (2002). Three-dimensional high-resolution second-harmonic generation imaging of endogenous structural proteins in biological tissues. *Biophys. J.* **82**, 493-508.

Canel, M., Serrels, A., Miller, D., Timpson, P., Serrels, B., Frame, M. C. and Brunton, V. G. (2010). Quantitative in vivo imaging of the effects of inhibiting integrin signaling via Src and FAK on cancer cell movement: effects on E-cadherin dynamics. *Cancer Res.* **70**, 9413-9422.

Cao, L., Kobayakawa, S., Yoshiki, A. and Abe, K. (2012). High resolution intravital imaging of subcellular structures of mouse abdominal organs using a microstage device. *PLoS ONE* **7**, e33876.

Caroline Müllenbroich, M., Mcghee, E. J., Wright, A. J., Anderson, K. I. and Mathieson, K. (2014). Strategies to overcome photobleaching in algorithm-based adaptive optics for nonlinear *in-vivo* imaging. *J. Biomed. Opt.* **19**, 016021.

Carpenter, A. E., Jones, T. R., Lamprecht, M. R., Clarke, C., Kang, I. H., Friman, O., Guertin, D. A., Chang, J. H., Lindquist, R. A., Moffat, J. et al. (2006). CellProfiler: image analysis software for identifying and quantifying cell phenotypes. *Genome Biol.* **7**, R100.

Chalfie, M., Tu, Y., Euskirchen, G., Ward, W. W. and Prasher, D. C. (1994). Green fluorescent protein as a marker for gene expression. *Science* **263**, 802-805.

Chang, J., Lucas, M. C., Leonte, L. E., Garcia-Montolio, M., Singh, L. B., Findlay, A. D., Deodhar, M., Foot, J. S., Jarolimek, W., Timpson, P. et al. (2017). Pre-clinical evaluation of small molecule LOXL2 inhibitors in breast cancer. *Oncotarget* **8**, 26066-26078.

Chen, Y., Aguirre, A. D., Hsiung, P. L., Desai, S., Herz, P. R., Pedrosa, M., Huang, Q., Figueiredo, M., Huang, S.-W., Koski, A. et al. (2007). Ultrahigh resolution optical coherence tomography of Barrett's esophagus: preliminary descriptive clinical study correlating images with histology. *Endoscopy* **39**, 599-605.

Chen, S.-Y., Chen, S.-U., Wu, H.-Y., Lee, W.-J., Liao, Y.-H. and Sun, C.-K. (2010). In vivo virtual biopsy of human skin by using noninvasive higher harmonic generation microscopy. *IEEE J. Sel. Top. Quantum Electron.* **16**, 478-492.

Chen, X., Lee, D., Yu, S., Kim, G., Lee, S., Cho, Y., Jeong, H., Nam, K. T. and Yoon, J. (2017). In vivo near-infrared imaging and phototherapy of tumors using a cathepsin B-activated fluorescent probe. *Biomaterials* **122**, 130-140.

Cheng, S., Cuenca, R. M., Liu, B., Malik, B. H., Jabbour, J. M., Maitland, K. C., Wright, J., Cheng, Y.-S. L. and Jo, J. A. (2014). Handheld multispectral fluorescence lifetime imaging system for in vivo applications. *Biomed. Opt. Express* **5**, 921-931.

Chittajallu, D. R., Florian, S., Kohler, R. H., Iwamoto, Y., Orth, J. D., Weissleder, R., Danuser, G. and Mitchison, T. J. (2015). In vivo cell-cycle profiling in xenograft tumors by quantitative intravital microscopy. *Nat. Methods* **12**, 577-585.

Choi, P. J. and Mitchison, T. J. (2013). Imaging burst kinetics and spatial coordination during serial killing by single natural killer cells. *Proc. Natl. Acad. Sci. USA* **110**, 6488-6493.

Chu, D., Dong, X., Zhao, Q., Gu, J. and Wang, Z. (2017). Photosensitization priming of tumor microenvironments improves delivery of nanotherapeutics via neutrophil infiltration. *Adv. Mater.* **29**, 1701021.

Chung, K. and Deisseroth, K. (2013). CLARITY for mapping the nervous system. *Nat. Methods* **10**, 508-513.

Cicchi, R., Kapsokalyvas, D., De Giorgi, V., Maio, V., Van Wiechen, A., Massi, D., Lotti, T. and Pavone, F. S. (2010). Scoring of collagen organization in healthy and diseased human dermis by multiphoton microscopy. *J. Biophotonics* **3**, 34-43.

Coffey, S. E., Giedt, R. J. and Weissleder, R. (2013). Automated analysis of clonal cancer cells by intravital imaging. *Intravital* **2**, e26138.

Conway, J. R. W., Carragher, N. O. and Timpson, P. (2014). Developments in preclinical cancer imaging: innovating the discovery of therapeutics. *Nat. Rev. Cancer* **14**, 314-328.

Conway, J. R. W., Warren, S. C. and Timpson, P. (2017). Context-dependent intravital imaging of therapeutic response using intramolecular FRET biosensors. *Methods* **128**, 78-94.

Costa-Silva, B., Aiello, N. M., Ocean, A. J., Singh, S., Zhang, H., Thakur, B. K., Becker, A., Hoshino, A., Mark, M. T., Molina, H. et al. (2015). Pancreatic cancer exosomes initiate pre-metastatic niche formation in the liver. *Nat. Cell Biol.* **17**, 816-826.

Davalos, D., Lee, J. K., Smith, W. B., Brinkman, B., Ellisman, M. H., Zheng, B. and Akassoglou, K. (2008). Sgtable in vivo imaging of densely populated glia, axons and blood vessels in the mouse spinal cord using two-photon microscopy. *J. Neurosci. Methods* **169**, 1-7.

de Beco, S., Gueudry, C., Amblard, F. and Coscoy, S. (2009). Endocytosis is required for E-cadherin redistribution at mature adherens junctions. *Proc. Natl. Acad. Sci. USA* **106**, 7010-7015.

de Boer, P., Hoogenboom, J. P. and Giepmans, B. N. G. (2015). Correlated light and electron microscopy: ultrastructure lights up! *Nat. Methods* **12**, 503-513.

de Chaumont, F., Dallongeville, S., Chenouard, N., Hervé, N., Pop, S., Provoost, T., Meas-Yedid, V., Pankajakshan, P., Lecomte, T., Le Montagner, Y. et al. (2012). Icy: an open bioimage informatics platform for extended reproducible research. *Nat. Methods* **9**, 690-696.

Débarre, D., Botcherby, E. J., Watanabe, T., Srinivas, S., Booth, M. J. and Wilson, T. (2009). Image-based adaptive optics for two-photon microscopy. *Opt. Lett.* **34**, 2495-2497.

Demeautis, C., Sipieter, F., Roul, J., Chapuis, C., Padilla-Parra, S., Riquet, F. B. and Tramier, M. (2017). Multiplexing PKA and ERK1&2 kinases FRET biosensors in living cells using single excitation wavelength dual colour FLIM. *Sci. Rep.* **7**, 41026.

Digman, M. A., Caiolfa, V. R., Zamai, M. and Gratton, E. (2008). The phasor approach to fluorescence lifetime imaging analysis. *Biophys. J.* **94**, L14-L16.

Dubach, J. M., Kim, E., Yang, K., Cuccarese, M., Giedt, R. J., Meimetis, L. G., Vinegoni, C. and Weissleder, R. (2017). Quantitating drug-target engagement in single cells in vitro and in vivo. *Nat. Chem. Biol.* **13**, 168-173.

Dunham, S. M., Pudavar, H. E., Prasad, P. N. and Stachowiak, M. K. (2004). Cellular signaling and protein-protein interactions studied using fluorescence recovery after photobleaching. *J. Phys. Chem. B* **108**, 10540-10546.

Edelstein, A. D., Tsuchida, M. A., Amodaj, N., Pinkard, H., Vale, R. D. and Stuurman, N. (2014). Advanced methods of microscope control using μManager software. *J. Biol. Methods* **1**, e10.

Ellenbroek, S. I. J. and Van Rheenen, J. (2014). Imaging hallmarks of cancer in living mice. *Nat. Rev. Cancer* **14**, 406-418.

Erami, Z., Herrmann, D., Warren, S. C., Nobis, M., Mcghee, E. J., Lucas, M. C., Leung, W., Reischmann, N., Mrowinska, A., Schwarz, J. P. et al. (2016). Intravital FRAP imaging using an E-cadherin-GFP mouse reveals disease- and drug-dependent dynamic regulation of cell-cell junctions in live tissue. *Cell Rep.* **14**, 152-167.

Evans, C. L. and Xie, X. S. (2008). Coherent anti-stokes raman scattering microscopy: chemical imaging for biology and medicine. *Annu. Rev. Anal. Chem.* **1**, 883-909.

Evans, C. L., Xu, X. Y., Kesari, S., Xie, X. S., Wong, S. T. C. and Young, G. S. (2007). Chemically-selective imaging of brain structures with CARS microscopy. *Opt. Express* **15**, 12076-12087.

Farnsworth, N. L., Hemmati, A., Pozzoli, M. and Benninger, R. K. P. (2014). Fluorescence recovery after photobleaching reveals regulation and distribution of connexin36 gap junction coupling within mouse islets of Langerhans. *J. Physiol.* **592**, 4431-4446.

Fehr, M., Lalonde, S., Lager, I., Wolff, M. W. and Frommer, W. B. (2003). In vivo imaging of the dynamics of glucose uptake in the cytosol of COS-7 cells by fluorescent nanosensors. *J. Biol. Chem.* **278**, 19127-19133.

Fiole, D., Deman, P., Trescos, Y., Mayol, J.-F., Mathieu, J., Vial, J.-C., Douady, J. and Tournier, J.-N. (2014). Two-photon intravital imaging of lungs during anthrax infection reveals long-lasting macrophage-dendritic cell contacts. *Infect. Immun.* **82**, 864-872.

Fischer, I., Westphal, M., Rossbach, B., Bethke, N., Hariharan, K., Ullah, I., Reinke, P., Kurtz, A. and Stachelscheid, H. (2017). Comparative characterization of decellularized renal scaffolds for tissue engineering. *Biomed. Mater.* **12**, 045005.

Fisher, D. T., Muhitch, J. B., Kim, M., Doyen, K. C., Bogner, P. N., Evans, S. S. and Skitzki, J. J. (2016). Intraoperative intravital microscopy permits the study of human tumour vessels. *Nat. Commun.* **7**, 10684.

Follain, G., Mercier, L., Osmani, N., Harlepp, S. and Goetz, J. G. (2017). Seeing is believing - multi-scale spatio-temporal imaging towards in vivo cell biology. *J. Cell Sci.* **130**, 23-38.

Friedl, P. and Gilmour, D. (2009). Collective cell migration in morphogenesis, regeneration and cancer. *Nat. Rev. Mol. Cell Biol.* **10**, 445-457.

Fritzsche, M. and Charras, G. (2015). Dissecting protein reaction dynamics in living cells by fluorescence recovery after photobleaching. *Nat. Protoc.* **10**, 660-680.

Fumagalli, A., Drost, J., Suijkerbuijk, S. J. E., Van Boxtel, R., De Ligt, J., Offerhaus, G. J., Begthel, H., Beerling, E., Tan, E. H., Sansom, O. J. et al. (2017). Genetic dissection of colorectal cancer progression by orthotopic transplantation of engineered cancer organoids. *Proc. Natl. Acad. Sci. USA* **114**, E2357-E2364.

Gaggioli, C., Hooper, S., Hidalgo-Carcedo, C., Grosse, R., Marshall, J. F., Harrington, K. and Sahai, E. (2007). Fibroblast-led collective invasion of carcinoma cells with differing roles for RhoGTPases in leading and following cells. *Nat. Cell Biol.* **9**, 1392-1400.

Galanzha, E. I., Viegas, M. G., Malinsky, T. I., Melerzanov, A. V., Juratli, M. A., Sarimollaoglu, M., Nedosekin, D. A. and Zharov, V. P. (2016). In vivo acoustic and photoacoustic focusing of circulating cells. *Sci. Rep.* **6**, 21531.

Galletly, N. P., Mcginty, J., Dunsby, C., Teixeira, F., Requejo-Isidro, J., Munro, I., Elson, D. S., Neil, M. A. A., Chu, A. C., French, P. M. W. et al. (2008). Fluorescence lifetime imaging distinguishes basal cell carcinoma from surrounding uninvolved skin. *Br. J. Dermatol.* **159**, 152-161.

Ghosh, K. K., Burns, L. D., Cocker, E. D., Nimmerjahn, A., Ziv, Y., Gamal, A. E. and Schnitzer, M. J. (2011). Miniaturized integration of a fluorescence microscope. *Nat. Methods* **8**, 871-878.

Giepmans, B. N. G., Adams, S. R., Ellisman, M. H. and Tsien, R. Y. (2006). The fluorescent toolbox for assessing protein location and function. *Science* **312**, 217-224.

Gligorijevic, B., Bergman, A. and Condeelis, J. (2014). Multiparametric classification links tumor microenvironments with tumor cell phenotype. *PLoS Biol.* **12**, e1001995.

Goehring, N. W., Chowdhury, D., Hyman, A. A. and Grill, S. W. (2010). FRAP analysis of membrane-associated proteins: lateral diffusion and membrane-cytoplasmic exchange. *Biophys. J.* **99**, 2443-2452.

Gora, M. J., Sauk, J. S., Carruth, R. W., Gallagher, K. A., Suter, M. J., Nishioka, N. S., Kava, L. E., Rosenberg, M., Bouma, B. E. and Tearney, G. J. (2013). Tethered capsule endomicroscopy enables less invasive imaging of gastrointestinal tract microstructure. *Nat. Med.* **19**, 238-240.

Goto, A., Nakahara, I., Yamaguchi, T., Kamioka, Y., Sumiyama, K., Matsuda, M., Nakanishi, S. and Funabiki, K. (2015). Circuit-dependent striatal PKA and ERK signaling underlies rapid behavioral shift in mating reaction of male mice. *Proc. Natl. Acad. Sci. USA* **112**, 6718-6723.

Gregory, P. A., Bert, A. G., Paterson, E. L., Barry, S. C., Tsykin, A., Farshid, G., Vadas, M. A., Khew-Goodall, Y. and Goodall, G. J. (2008). The miR-200 family and miR-205 regulate epithelial to mesenchymal transition by targeting ZEB1 and SIP1. *Nat. Cell Biol.* **10**, 593-601.

Grey, A. C., Chaurand, P., Caprioli, R. M. and Schey, K. L. (2009). MALDI imaging mass spectrometry of integral membrane proteins from ocular lens and retinal tissue. *J. Proteome Res.* **8**, 3278-3283.

Haghayegh Jahromi, N., Tardent, H., Enzmann, G., Deutsch, U., Kawakami, N., Bittner, S., Vestweber, D., Zipp, F., Stein, J. V. and Engelhardt, B. (2017). A novel cervical spinal cord window preparation allows for two-photon imaging of T-cell interactions with the cervical spinal cord microvasculature during experimental autoimmune encephalomyelitis. *Front. Immunol.* **8**, 406.

Hampton, H. R., Bailey, J., Tomura, M., Brink, R. and Chtanova, T. (2015). Microbe-dependent lymphatic migration of neutrophils modulates lymphocyte proliferation in lymph nodes. *Nat. Commun.* **6**, 7139.

Harney, A. S., Arwert, E. N., Entenberg, D., Wang, Y., Guo, P., Qian, B.-Z., Oktay, M. H., Pollard, J. W., Jones, J. G. and Condeelis, J. S. (2015). Real-time imaging reveals local, transient vascular permeability, and tumor cell intravasation stimulated by TIE2(hi) macrophage-derived VEGFA. *Cancer Discov.* **5**, 932-943.

Harpel, K., Baker, R. D., Amirsolaimani, B., Mehravar, S., Vagner, J., Matsunaga, T. O., Banerjee, B. and Kieu, K. (2016). Imaging of targeted lipid microbubbles to detect cancer cells using third harmonic generation microscopy. *Biomed. Opt. Express* **7**, 2849-2859.

Harvey, C. D., Ehrhardt, A. G., Cellurale, C., Zhong, H., Yasuda, R., Davis, R. J. and Svoboda, K. (2008). A genetically encoded fluorescent sensor of ERK activity. *Proc. Natl. Acad. Sci. USA* **105**, 19264-19269.

Hawkins, E. D., Duarte, D., Akinduro, O., Khorshed, R. A., Passaro, D., Nowicka, M., Straszkowski, L., Scott, M. K., Rothery, S., Ruivo, N. et al. (2016). T-cell acute leukaemia exhibits dynamic interactions with bone marrow microenvironments. *Nature* **538**, 518.

Headley, M. B., Bins, A., Nip, A., Roberts, E. W., Looney, M. R., Gerard, A. and Krummel, M. F. (2016). Visualization of immediate immune responses to pioneer metastatic cells in the lung. *Nature* **531**, 513-517.

Held, M., Schmitz, M. H. A., Fischer, B., Walter, T., Neumann, B., Olma, M. H., Peter, M., Ellenberg, J. and Gerlich, D. W. (2010). CellCognition: time-resolved phenotype annotation in high-throughput live cell imaging. *Nat. Methods* **7**, 747-754.

Heuke, S., Vogler, N., Meyer, T., Akimov, D., Kluschke, F., Röwert-Huber, H.-J., Lademann, J., Dietzek, B. and Popp, J. (2013). Detection and discrimination of non-melanoma skin cancer by multimodal imaging. *Healthcare (Basel)* **1**, 64-83.

Hind, L. E., Vincent, W. J. B. and Huttenlocher, A. (2016). Leading from the back: the role of the uropod in neutrophil polarization and migration. *Dev. Cell* **38**, 161-169.

Hirata, E., Girotti, M. R., Viros, A., Hooper, S., Spencer-Dene, B., Matsuda, M., Larkin, J., Marais, R. and Sahai, E. (2015). Intravital imaging reveals how BRAF inhibition generates drug-tolerant microenvironments with high integrin beta1/FAK signaling. *Cancer Cell* **27**, 574-588.

Hiratsuka, T., Fujita, Y., Naoki, H., Aoki, K., Kamioka, Y. and Matsuda, M. (2015). Intercellular propagation of extracellular signal-regulated kinase activation revealed by in vivo imaging of mouse skin. *Elife* **4**, e05178.

Hoshino, A., Costa-Silva, B., Shen, T.-L., Rodrigues, G., Hashimoto, A., Tesic Mark, M., Molina, H., Kohsaka, S., Di Giannatale, A., Ceder, S. et al. (2015). Tumour exosome integrins determine organotropic metastasis. *Nature* **527**, 329-335.

Huang, P., Song, H., Zhang, Y., Liu, J., Zhang, J., Wang, W., Liu, J., Li, C. and Kong, D. (2016a). Bridging the gap between macroscale drug delivery systems and nanomedicines: a nanoparticle-assembled thermosensitive hydrogel for peritumoral chemotherapy. *ACS Appl. Mater. Interfaces* **8**, 29323-29333.

Huang, Y., Qiu, F., Shen, L., Chen, D., Su, Y., Yang, C., Li, B., Yan, D. and Zhu, X. (2016b). Combining two-photon-activated fluorescence resonance energy transfer and near-infrared photothermal effect of unimolecular micelles for enhanced photodynamic therapy. *ACS Nano* **10**, 10489-10499.

Huck, V., Gorzelanny, C., Thomas, K., Getova, V., Niemeyer, V., Zens, K., Unnerstall, T. R., Feger, J. S., Fallah, M. A., Metze, D. et al. (2016). From morphology to biochemical state - intravital multiphoton fluorescence lifetime imaging of inflamed human skin. *Sci. Rep.* **6**, 22789.

Huo, C. W., Chew, G., Hill, P., Huang, D., Ingman, W., Hodson, L., Brown, K. A., Magenau, A., Allam, A. H., McGhee, E. et al. (2015). High mammographic density is associated with an increase in stromal collagen and immune cells within the mammary epithelium. *Breast Cancer Res.* **17**, 79.

Ilhan-Mutlu, A., Osswald, M., Liao, Y., Gommel, M., Reck, M., Miles, D., Mariani, P., Gianni, L., Lutiger, B., Nendel, V. et al. (2016). Bevacizumab prevents brain metastases formation in lung adenocarcinoma. *Mol. Cancer Ther.* **15**, 702-710.

Ilina, O. and Friedl, P. (2009). Mechanisms of collective cell migration at a glance. *J. Cell Sci.* **122**, 3203-3208.

Imamura, H., Huynh Nhat, K. P., Togawa, H., Saito, K., Iino, R., Kato-Yamada, Y., Nagai, T. and Noji, H. (2009). Visualization of ATP levels inside single living cells with fluorescence resonance energy transfer-based genetically encoded indicators. *Proc. Natl. Acad. Sci. USA* **106**, 15651-15656.

Janssen, A., Beerling, E., Medema, R. and Van Rheenen, J. (2013). Intravital FRET imaging of tumor cell viability and mitosis during chemotherapy. *PLoS ONE* **8**, e64029.

Ji, N., Sato, T. R. and Betzig, E. (2012). Characterization and adaptive optical correction of aberrations during in vivo imaging in the mouse cortex. *Proc. Natl. Acad. Sci. USA* **109**, 22-27.

Johnsson, A.-K. E., Dai, Y., Nobis, M., Baker, M. J., Mcghee, E. J., Walker, S., Schwarz, J. P., Kadir, S., Morton, J. P., Myant, K. B. et al. (2014). The Rac-FRET mouse reveals tight spatiotemporal control of Rac activity in primary cells and tissues. *Cell Rep.* **6**, 1153-1164.

Junankar, S., Shay, G., Jurczyluk, J., Ali, N., Down, J., Pocock, N., Parker, A., Nguyen, A., Sun, S., Kashemirov, B. et al. (2015). Real-time intravital imaging establishes tumor-associated macrophages as the extraskeletal target of bisphosphonate action in cancer. *Cancer Discov.* **5**, 35-42.

Jung, E., Osswald, M., Blaes, J., Wiestler, B., Sahm, F., Schmenger, T., Solecki, G., Deumelandt, K., Kurz, F. T., Xie, R. et al. (2017). Tweety-homolog 1 drives brain colonization of gliomas. *J. Neurosci.* **37**, 6837-6850.

Jusu, S., Presley, J. F. and Kremer, R. (2017). Phosphorylation of human retinoid X receptor alpha at serine 260 impairs its subcellular localization, receptor interaction, nuclear mobility, and 1alpha,25-dihydroxyvitamin D3-dependent DNA binding in Ras-transformed keratinocytes. *J. Biol. Chem.* **292**, 1490-1509.

Kalinina, S., Breymayer, J., Schäfer, P., Calzia, E., Shcheslavskiy, V., Becker, W. and Rück, A. (2016). Correlative NAD(P)H-FLIM and oxygen sensing-PLIM for metabolic mapping. *J. Biophotonics* **9**, 800-811.

Kamerkar, S., LeBleu, V. S., Sugimoto, H., Yang, S., Ruivo, C. F., Melo, S. A., Lee, J. J. and Kalluri, R. (2017). Exosomes facilitate therapeutic targeting of oncogenic KRAS in pancreatic cancer. *Nature* **546**, 498-503.

Kamioka, Y., Sumiyama, K., Mizuno, R., Sakai, Y., Hirata, E., Kiyokawa, E. and Matsuda, M. (2012). Live imaging of protein kinase activities in transgenic mice expressing FRET biosensors. *Cell Struct. Funct.* **37**, 65-73.

Karagiannis, G. S., Pastoriza, J. M., Wang, Y., Harney, A. S., Entenberg, D., Pignatelli, J., Sharma, V. P., Xue, E. A., Cheng, E., D'Alfonso, T. M. et al. (2017). Neoadjuvant chemotherapy induces breast cancer metastasis through a TMEM-mediated mechanism. *Sci. Transl. Med.* **9**, eaan0026.

Kardash, E., Reichman-Fried, M., Maître, J.-L., Boldajipour, B., Papusheva, E., Messerschmidt, E.-M., Heisenberg, C.-P. and Raz, E. (2010). A role for Rho GTPases and cell-cell adhesion in single-cell motility in vivo. *Nat. Cell Biol.* **12**, 47-53; sup pp 1-11.

Karl, A., Stepp, H., Willmann, E., Buchner, A., Hocaoglu, Y., Stief, C. and Tritschler, S. (2010). Optical coherence tomography for bladder cancer - ready as a surrogate for optical biopsy? - results of a prospective mono-centre study. *Eur. J. Med. Res.* **15**, 131-134.

Karreman, M. A., Hyenne, V., Schwab, Y. and Goetz, J. G. (2016a). Intravital correlative microscopy: imaging life at the nanoscale. *Trends Cell Biol.* **26**, 848-863.

Karreman, M. A., Mercier, L., Schieber, N. L., Solecki, G., Allio, G., Winkler, F., Ruthensteiner, B., Goetz, J. G. and Schwab, Y. (2016b). Fast and precise targeting of single tumor cells in vivo by multimodal correlative microscopy. *J. Cell Sci.* **129**, 444-456.

Kasischke, K. A., Lambert, E. M., Panepento, B., Sun, A., Gelbard, H. A., Burgess, R. W., Foster, T. H. and Nedergaard, M. (2011). Two-photon NADH

imaging exposes boundaries of oxygen diffusion in cortical vascular supply regions. *J. Cereb. Blood Flow Metab.* **31**, 68-81.

Kedrin, D., Gligorijevic, B., Wyckoff, J., Verkhusha, V. V., Condeelis, J., Segall, J. E. and Van Rheenen, J. (2008). Intravital imaging of metastatic behavior through a mammary imaging window. *Nat. Methods* **5**, 1019-1021.

Keller, P. J., Schmidt, A. D., Wittbrodt, J. and Stelzer, E. H. K. (2008). Reconstruction of zebrafish early embryonic development by scanned light sheet microscopy. *Science* **322**, 1065-1069.

Khait, I., Orsher, Y., Golan, O., Binshtok, U., Gordon-Bar, N., Amir-Zilberstein, L. and Sprinzak, D. (2016). Quantitative analysis of delta-like 1 membrane dynamics elucidates the role of contact geometry on Notch signaling. *Cell Rep.* **14**, 225-233.

Khorshed, R. A., Hawkins, E. D., Duarte, D., Scott, M. K., Akinduro, O. A., Rashidi, N. M., Spitaler, M. and Lo Celso, C. (2015). Automated identification and localization of hematopoietic stem cells in 3D intravital microscopy data. *Stem Cell Rep.* **5**, 139-153.

Kim, C. S., Wilder-Smith, P. B. B., Ahn, Y.-C., Liaw, L.-H. L., Chen, Z. and Kwon, Y. J. (2009). Enhanced detection of early-stage oral cancer in vivo by optical coherence tomography using multimodal delivery of gold nanoparticles. *J. Biomed. Opt.* **14**, 034008.

Kim, J. V., Jiang, N., Tadokoro, C. E., Liu, L., Ransohoff, R. M., Lafaille, J. J. and Dustin, M. L. (2010). Two-photon laser scanning microscopy imaging of intact spinal cord and cerebral cortex reveals requirement for CXCR6 and neuroinflammation in immune cell infiltration of cortical injury sites. *J. Immunol. Methods* **352**, 89-100.

Kirkpatrick, N., Chung, E., Cook, D., Han, X., Gruionu, G., Liao, S., Munn, L., Padera, T., Fukumura, D. and Jain, R. K. (2012). Video-rate resonant scanning multiphoton microscopy: An emerging technique for intravital imaging of the tumor microenvironment. *Intravital* **1**, 60-68.

Koenig, K. and Riemann, I. (2003). High-resolution multiphoton tomography of human skin with subcellular spatial resolution and picosecond time resolution. *J. Biomed. Opt.* **8**, 432-439.

Kraft, L. J., Dowler, J. and Kenworthy, A. K. (2014). Frap-Toolbox: Software for the analysis of fluorescence recovery after photobleaching [Online]. Available at: http://www.fraptoolbox.com.

Kular, J., Scheer, K. G., Pyne, N. T., Allam, A. H., Pollard, A. N., Magenau, A., Wright, R. L., Kolesnikoff, N., Moretti, P. A., Wullkopf, L. et al. (2015). A negative regulatory mechanism involving 14-3-3zeta limits signaling downstream of ROCK to regulate tissue stiffness in epidermal homeostasis. *Dev. Cell* **35**, 759-774.

Kumagai, Y., Naoki, H., Nakasyo, E., Kamioka, Y., Kiyokawa, E. and Matsuda, M. (2015). Heterogeneity in ERK activity as visualized by in vivo FRET imaging of mammary tumor cells developed in MMTV-Neu mice. *Oncogene* **34**, 1051-1057.

Kumar, A., Ouyang, M., Van Den Dries, K., Mcghee, E. J., Tanaka, K., Anderson, M. D., Groisman, A., Goult, B. T., Anderson, K. I. and Schwartz, M. A. (2016). Talin tension sensor reveals novel features of focal adhesion force transmission and mechanosensitivity. *J. Cell Biol.* **213**, 371-383.

Kuzmin, N. V., Wesseling, P., Hamer, P. C. W., Noske, D. P., Galgano, G. D., Mansvelder, H. D., Baayen, J. C. and Groot, M. L. (2016). Third harmonic generation imaging for fast, label-free pathology of human brain tumors. *Biomed. Opt. Express* **7**, 1889-1904.

Kvilekval, K., Fedorov, D., Obara, B., Singh, A. and Manjunath, B. S. (2010). Bisque: a platform for bioimage analysis and management. *Bioinformatics* **26**, 544-552.

Labernadie, A., Kato, T., Brugués, A., Serra-Picamal, X., Derzsi, S., Arwert, E., Weston, A., González-Tarragó, V., Elosegui-Artola, A., Albertazzi, L. et al. (2017). A mechanically active heterotypic E-cadherin/N-cadherin adhesion enables fibroblasts to drive cancer cell invasion. *Nat. Cell Biol.* **19**, 224-237.

Langer, D., van 'T Hoff, M., Keller, A. J., Nagaraja, C., Pfäffli, O. A., Göldi, M., Kasper, H. and Helmchen, F. (2013). HelioScan: a software framework for controlling in vivo microscopy setups with high hardware flexibility, functional diversity and extendibility. *J. Neurosci. Methods* **215**, 38-52.

Laughney, A. M., Kim, E., Sprachman, M. M., Miller, M. A., Kohler, R. H., Yang, K. S., Orth, J. D., Mitchison, T. J. and Weissleder, R. (2014). Single-cell pharmacokinetic imaging reveals a therapeutic strategy to overcome drug resistance to the microtubule inhibitor eribulin. *Sci. Transl. Med.* **6**, 261ra152.

Laviv, T., Kim, B. B., Chu, J., Lam, A. J., Lin, M. Z. and Yasuda, R. (2016). Simultaneous dual-color fluorescence lifetime imaging with novel red-shifted fluorescent proteins. *Nat. Methods* **13**, 989-992.

Le, T. T., Rehrer, C. W., Huff, T. B., Nichols, M. B., Camarillo, I. G. and Cheng, J. X. (2007). Nonlinear optical imaging to evaluate the impact of obesity on mammary gland and tumor stroma. *Mol. Imaging* **6**, 205-211.

Le, T. T., Huff, T. B. and Cheng, J.-X. (2009). Coherent anti-Stokes Raman scattering imaging of lipids in cancer metastasis. *BMC Cancer* **9**, 42.

Le, V.-H., Lee, S., Lee, S., Wang, T., Jang, W. H., Yoon, Y., Kwon, S., Kim, H., Lee, S.-W. and Kim, K. H. (2017). In vivo longitudinal visualization of bone marrow engraftment process in mouse calvaria using two-photon microscopy. *Sci. Rep.* **7**, 44097.

Le Devedec, S. E., Geverts, B., De Bont, H., Yan, K., Verbeek, F. J., Houtsmuller, A. B. and Van De Water, B. (2012). The residence time of focal adhesion kinase (FAK) and paxillin at focal adhesions in renal epithelial cells is determined by adhesion size, strength and life cycle status. *J. Cell Sci.* **125**, 4498-4506.

Lee, M. and Serrels, A. (2016). Multiphoton Microscopy for Visualizing Lipids in Tissue. *Methods Mol. Biol.* **1467**, 105-118.

Lee, S., Vinegoni, C., Weissleder, R. and Feruglio, P. F. (2012). Improved intravital microscopy via synchronization of respiration and holder stabilization. *J. Biomed. Opt.* **17**, 096018.

Lee, S., Vinegoni, C., Sebas, M. and Weissleder, R. (2014). Automated motion artifact removal for intravital microscopy, without a priori information. *Sci. Rep.* **4**, 4507.

Lee, M., Downes, A., Chau, Y.-Y., Serrels, B., Hastie, N., Elfick, A., Brunton, V., Frame, M. and Serrels, A. (2015). In vivo imaging of the tumor and its associated microenvironment using combined CARS / 2-photon microscopy. *Intravital* **4**, e1055430.

Lefrançais, E., Ortiz-Muñoz, G., Caudrillier, A., Mallavia, B., Liu, F., Sayah, D. M., Thornton, E. E., Headley, M. B., David, T., Coughlin, S. R. et al. (2017). The lung is a site of platelet biogenesis and a reservoir for haematopoietic progenitors. *Nature* **544**, 105-109.

Légaré, F., Evans, C. L., Ganikhanov, F. and Xie, X. S. (2006). Towards CARS endoscopy. *Opt. Express* **14**, 4427-4432.

Lehmann, S., Perera, R., Grimm, H.-P., Sam, J., Colombetti, S., Fauti, T., Fahrni, L., Schaller, T., Freimoser-Grundschober, A., Zielonka, J. et al. (2016a). In vivo fluorescence imaging of the activity of CEA TCB, a novel T-cell bispecific antibody, reveals highly specific tumor targeting and fast induction of T-cell-mediated tumor killing. *Clin. Cancer Res.* **22**, 4417-4427.

Lehmann, W., Mossmann, D., Kleemann, J., Mock, K., Meisinger, C., Brummer, T., Herr, R., Brabletz, S., Stemmler, M. P. and Brabletz, T. (2016b). ZEB1 turns into a transcriptional activator by interacting with YAP1 in aggressive cancer types. *Nat. Commun.* **7**, 10498.

Li, G., Liu, T., Tarokh, A., Nie, J., Guo, L., Mara, A., Holley, S. and Wong, S. T. C. (2007). 3D cell nuclei segmentation based on gradient flow tracking. *BMC Cell Biol.* **8**, 40.

Li, J. L. Y., Lim, C. H., Tay, F. W., Goh, C. C., Devi, S., Malleret, B., Lee, B., Bakocevic, N., Chong, S. Z., Evrard, M. et al. (2016a). Neutrophils self-regulate immune complex-mediated cutaneous inflammation through CXCL2. *J. Investig. Dermatol.* **136**, 416-424.

Li, K., Xiang, X., Sun, J., He, H.-T., Wu, J., Wang, Y. and Zhu, C. (2016b). Imaging spatiotemporal activities of ZAP-70 in live T cells using a FRET-based biosensor. *Ann. Biomed. Eng.* **44**, 3510-3521.

Li, S., Zhang, Y., Wang, J., Zhao, Y., Ji, T., Zhao, X., Ding, Y., Zhao, X., Zhao, R., Li, F. et al. (2017). Nanoparticle-mediated local depletion of tumour-associated platelets disrupts vascular barriers and augments drug accumulation in tumours. *Nat. Biomed. Eng.* **1**, 667-679.

Liao, Y.-H., Chen, S.-Y., Chou, S.-Y., Wang, P.-H., Tsai, M.-R. and Sun, C.-K. (2013). Determination of chronological aging parameters in epidermal keratinocytes by in vivo harmonic generation microscopy. *Biomed. Opt. Express* **4**, 77-88.

Lin, E. Y., Jones, J. G., Li, P., Zhu, L., Whitney, K. D., Muller, W. J. and Pollard, J. W. (2003). Progression to malignancy in the polyoma middle T oncoprotein mouse breast cancer model provides a reliable model for human diseases. *Am. J. Pathol.* **163**, 2113-2126.

Liu, T., Yamaguchi, Y., Shirasaki, Y., Shikada, K., Yamagishi, M., Hoshino, K., Kaisho, T., Takemoto, K., Suzuki, T., Kuranaga, E. et al. (2014). Single-cell imaging of caspase-1 dynamics reveals an all-or-none inflammasome signaling response. *Cell Rep.* **8**, 974-982.

Liu, Y., Gu, Y., Han, Y., Zhang, Q., Jiang, Z., Zhang, X., Huang, B., Xu, X., Zheng, J. and Cao, X. (2016). Tumor exosomal RNAs promote lung pre-metastatic niche formation by activating alveolar epithelial TLR3 to recruit neutrophils. *Cancer Cell* **30**, 243-256.

Machado, M. J. C. and Mitchell, C. A. (2011). Temporal changes in microvessel leakiness during wound healing discriminated by in vivo fluorescence recovery after photobleaching. *J. Physiol.* **589**, 4681-4696.

Mächler, P., Wyss, M. T., Elsayed, M., Stobart, J., Gutierrez, R., Von Faber-Castell, A., Kaelin, V., Zuend, M., San Martín, A., Romero-Gómez, I. et al. (2016). In vivo evidence for a lactate gradient from astrocytes to neurons. *Cell Metab.* **23**, 94-102.

Malik, B. H., Lee, J., Cheng, S., Cuenca, R., Jabbour, J. M., Cheng, Y.-S. L., Wright, J. M., Ahmed, B., Maitland, K. C. and Jo, J. A. (2016). Objective detection of oral carcinoma with multispectral fluorescence lifetime imaging in vivo. *Photochem. Photobiol.* **92**, 694-701.

Manning, C. S., Hooper, S. and Sahai, E. A. (2015). Intravital imaging of SRF and Notch signalling identifies a key role for EZH2 in invasive melanoma cells. *Oncogene* **34**, 4320-4332.

Marée, R., Rollus, L., Stévens, B., Hoyoux, R., Louppe, G., Vandaele, R., Begon, J.-M., Kainz, P., Geurts, P. and Wehenkel, L. (2016). Collaborative analysis of multi-gigapixel imaging data using Cytomine. *Bioinformatics* **32**, 1395-1401.

Martínez-Moreno, M., Leiva, M., Aguilera-Montilla, N., Sevilla-Movilla, S., Isern de Val, S., Arellano-Sanchez, N., Gutiérrez, N. C., Maldonado, R., Martínez-López, J., Buño, I. et al. (2016). In vivo adhesion of malignant B cells to bone

marrow microvasculature is regulated by alpha 4 beta 1 cytoplasmic-binding proteins. *Leukemia* **30**, 861-872.
Masedunskas, A., Chen, Y., Stussman, R., Weigert, R. and Mather, I. H. (2017). Kinetics of milk lipid droplet transport, growth, and secretion revealed by intravital imaging: lipid droplet release is intermittently stimulated by oxytocin. *Mol. Biol. Cell* **28**, 935-946.
Masuzzo, P., Van Troys, M., Ampe, C. and Martens, L. (2016). Taking aim at moving targets in computational cell migration. *Trends Cell Biol.* **26**, 88-110.
Matsumoto, Y., Nomoto, T., Cabral, H., Matsumoto, Y., Watanabe, S., Christie, R. J., Miyata, K., Oba, M., Ogura, T., Yamasaki, Y. et al. (2010). Direct and instantaneous observation of intravenously injected substances using intravital confocal micro-videography. *Biomed. Opt. Express* **1**, 1209-1216.
Matsumoto, Y., Nichols, J. W., Toh, K., Nomoto, T., Cabral, H., Miura, Y., Christie, R. J., Yamada, N., Ogura, T., Kano, M. R. et al. (2016). Vascular bursts enhance permeability of tumour blood vessels and improve nanoparticle delivery. *Nat. Nanotechnol.* **11**, 533-538.
Mayorca-Guiliani, A. E., Madsen, C. D., Cox, T. R., Horton, E. R., Venning, F. A. and Erler, J. T. (2017). ISDoT: in situ decellularization of tissues for high-resolution imaging and proteomic analysis of native extracellular matrix. *Nat. Med.* **23**, 890-898.
Meyer, T., Bergner, N., Bielecki, C., Krafft, C., Akimov, D., Romeike, B. F. M., Reichart, R., Kalff, R., Dietzek, B. and Popp, J. (2011). Nonlinear microscopy, infrared, and Raman microspectroscopy for brain tumor analysis. *J. Biomed. Opt.* **16**, 021113.
Meyer, T., Guntinas-Lichius, O., Von Eggeling, F., Ernst, G., Akimov, D., Schmitt, M., Dietzek, B. and Popp, J. (2013). Multimodal nonlinear microscopic investigations on head and neck squamous cell carcinoma: toward intraoperative imaging. *Head Neck* **35**, E280-E287.
Milberg, O., Shitara, A., Ebrahim, S., Masedunskas, A., Tora, M., Tran, D. T., Chen, Y., Conti, M. A., Adelstein, R. S., Ten Hagen, K. G. et al. (2017). Concerted actions of distinct nonmuscle myosin II isoforms drive intracellular membrane remodeling in live animals. *J. Cell Biol.* **216**, 1925-1936.
Miller, M. A. and Weissleder, R. (2017). Imaging of anticancer drug action in single cells. *Nat. Rev. Cancer* **17**, 399-414.
Miller, B. W., Morton, J. P., Pinese, M., Saturno, G., Jamieson, N. B., Mcghee, E., Timpson, P., Leach, J., Mcgarry, L., Shanks, E. et al. (2015). Targeting the LOX/hypoxia axis reverses many of the features that make pancreatic cancer deadly: inhibition of LOX abrogates metastasis and enhances drug efficacy. *EMBO Mol. Med.* **7**, 1063-1076.
Miller, M. A., Chandra, R., Cuccarese, M. F., Pfirschke, C., Engblom, C., Stapleton, S., Adhikary, U., Kohler, R. H., Mohan, J. F., Pittet, M. J. et al. (2017). Radiation therapy primes tumors for nanotherapeutic delivery via macrophage-mediated vascular bursts. *Sci. Transl. Med.* **9**, eaal0225.
Miyawaki, A., Llopis, J., Heim, R., Mccaffery, J. M., Adams, J. A., Ikura, M. and Tsien, R. Y. (1997). Fluorescent indicators for Ca2+ based on green fluorescent proteins and calmodulin. *Nature* **388**, 882-887.
Mizuno, R., Kamioka, Y., Kabashima, K., Imajo, M., Sumiyama, K., Nakasho, E., Ito, T., Hamazaki, Y., Okuchi, Y., Sakai, Y. et al. (2014). In vivo imaging reveals PKA regulation of ERK activity during neutrophil recruitment to inflamed intestines. *J. Exp. Med.* **211**, 1123-1136.
Mizuno, R., Kamioka, Y., Sakai, Y. and Matsuda, M. (2016). Visualization of signaling molecules during neutrophil recruitment in transgenic mice expressing FRET biosensors. *Methods Mol. Biol.* **1422**, 149-160.
Mochizuki, N., Yamashita, S., Kurokawa, K., Ohba, Y., Nagai, T., Miyawaki, A. and Matsuda, M. (2001). Spatio-temporal images of growth-factor-induced activation of Ras and Rap1. *Nature* **411**, 1065-1068.
Mukherjee, S., Jansen, V., Jikeli, J. F., Hamzeh, H., Alvarez, L., Dombrowski, M., Balbach, M., Strünker, T., Seifert, R., Kaupp, U. B. et al. (2016). A novel biosensor to study cAMP dynamics in cilia and flagella. *Elife* **5**, e14052.
Muriello, P. A. and Dunn, K. W. (2008). Improving signal levels in intravital multiphoton microscopy using an objective correction collar. *Opt. Commun.* **281**, 1806-1812.
Netti, P. A., Berk, D. A., Swartz, M. A., Grodzinsky, A. J. and Jain, R. K. (2000). Role of extracellular matrix assembly in interstitial transport in solid tumors. *Cancer Res.* **60**, 2497-2503.
Newman, R. H., Fosbrink, M. D. and Zhang, J. (2011). Genetically encodable fluorescent biosensors for tracking signaling dynamics in living cells. *Chem. Rev.* **111**, 3614-3666.
Nguyen, Q.-T., Callamaras, N., Hsieh, C. and Parker, I. (2001). Construction of a two-photon microscope for video-rate Ca(2+) imaging. *Cell Calcium* **30**, 383-393.
Nguyen, F. T., Zysk, A. M., Chaney, E. J., Kotynek, J. G., Oliphant, U. J., Bellafiore, F. J., Rowland, K. M., Johnson, P. A. and Boppart, S. A. (2009). Intraoperative evaluation of breast tumor margins with optical coherence tomography. *Cancer Res.* **69**, 8790-8796.
Niesner, R., Andresen, V., Neumann, J., Spiecker, H. and Gunzer, M. (2007). The power of single and multibeam two-photon microscopy for high-resolution and high-speed deep tissue and intravital imaging. *Biophys. J.* **93**, 2519-2529.
Nobis, M., Mcghee, E. J., Morton, J. P., Schwarz, J. P., Karim, S. A., Quinn, J., Edward, M., Campbell, A. D., Mcgarry, L. C., Evans, T. R. J. et al. (2013). Intravital FLIM-FRET imaging reveals dasatinib-induced spatial control of src in pancreatic cancer. *Cancer Res.* **73**, 4674-4686.
Nobis, M., Herrmann, D., Warren, S. C., Kadir, S., Leung, W., Killen, M., Magenau, A., Stevenson, D., Lucas, M. C., Reischmann, N. et al. (2017). A RhoA-FRET biosensor mouse for intravital imaging in normal tissue homeostasis and disease contexts. *Cell Rep.* **21**, 274-288.
Odoardi, F., Kawakami, N., Klinkert, W. E. F., Wekerle, H. and Flugel, A. (2007). Blood-borne soluble protein antigen intensifies T cell activation in autoimmune CNS lesions and exacerbates clinical disease. *Proc. Natl. Acad. Sci. USA* **104**, 18625-18630.
Okumoto, S., Looger, L. L., Micheva, K. D., Reimer, R. J., Smith, S. J. and Frommer, W. B. (2005). Detection of glutamate release from neurons by genetically encoded surface-displayed FRET nanosensors. *Proc. Natl. Acad. Sci. USA* **102**, 8740-8745.
Olivier, N., Aptel, F., Plamann, K., Schanne-Klein, M.-C. and Beaurepaire, E. (2010). Harmonic microscopy of isotropic and anisotropic microstructure of the human cornea. *Opt. Express* **18**, 5028-5040.
Onuki, R., Nagasaki, A., Kawasaki, H., Baba, T., Uyeda, T. Q. P. and Taira, K. (2002). Confirmation by FRET in individual living cells of the absence of significant amyloid beta -mediated caspase 8 activation. *Proc. Natl. Acad. Sci. USA* **99**, 14716-14721.
Orth, J. D., Kohler, R. H., Foijer, F., Sorger, P. K., Weissleder, R. and Mitchison, T. J. (2011). Analysis of mitosis and antimitotic drug responses in tumors by in vivo microscopy and single-cell pharmacodynamics. *Cancer Res.* **71**, 4608-4616.
Osswald, M. and Winkler, F. (2013). Insights into cell-to-cell and cell-to-blood-vessel communications in the brain: in vivo multiphoton microscopy. *Cell Tissue Res.* **352**, 149-159.
Osswald, M., Jung, E., Sahm, F., Solecki, G., Venkataramani, V., Blaes, J., Weil, S., Horstmann, H., Wiestler, B., Syed, M. et al. (2015). Brain tumour cells interconnect to a functional and resistant network. *Nature* **528**, 93-98.
Pantazis, P. and Supatto, W. (2014). Advances in whole-embryo imaging: a quantitative transition is underway. *Nat. Rev. Mol. Cell Biol.* **15**, 327-339.
Park, J., Wysocki, R. W., Amoozgar, Z., Maiorino, L., Fein, M. R., Jorns, J., Schott, A. F., Kinugasa-Katayama, Y., Lee, Y., Won, N. H. et al. (2016a). Cancer cells induce metastasis-supporting neutrophil extracellular DNA traps. *Sci. Transl. Med.* **8**, 361ra138.
Park, J. Y., Lee, J. Y., Zhang, Y., Hoffman, R. M. and Bouvet, M. (2016b). Targeting the insulin growth factor-1 receptor with fluorescent antibodies enables high resolution imaging of human pancreatic cancer in orthotopic mouse models. *Oncotarget* **7**, 18262-18268.
Patil, C. A., Bosschaart, N., Keller, M. D., Van Leeuwen, T. G. and Mahadevan-Jansen, A. (2008). Combined Raman spectroscopy and optical coherence tomography device for tissue characterization. *Opt. Lett.* **33**, 1135-1137.
Peinado, H., Zhang, H., Matei, I. R., Costa-Silva, B., Hoshino, A., Rodrigues, G., Psaila, B., Kaplan, R. N., Bromberg, J. F., Kang, Y. et al. (2017). Pre-metastatic niches: organ-specific homes for metastases. *Nat. Rev. Cancer* **17**, 302-317.
Pietraszewska-Bogiel, A. and Gadella, T. W. J. (2011). FRET microscopy: from principle to routine technology in cell biology. *J. Microsc.* **241**, 111-118.
Piston, D. W. and Kremers, G.-J. (2007). Fluorescent protein FRET: the good, the bad and the ugly. *Trends Biochem. Sci.* **32**, 407-414.
Plotnikov, S., Juneja, V., Isaacson, A. B., Mohler, W. A. and Campagnola, P. J. (2006). Optical clearing for improved contrast in second harmonic generation Imaging of skeletal muscle. *Biophys. J.* **90**, 328-339.
Pluen, A., Boucher, Y., Ramanujan, S., Mckee, T. D., Gohongi, T., Di Tomaso, E., Brown, E. B., Izumi, Y., Campbell, R. B., Berk, D. A. et al. (2001). Role of tumor-host interactions in interstitial diffusion of macromolecules: cranial vs. subcutaneous tumors. *Proc. Natl. Acad. Sci. USA* **98**, 4628-4633.
Pologruto, T. A., Sabatini, B. L. and Svoboda, K. (2003). ScanImage: flexible software for operating laser scanning microscopes. *Biomed. Eng. Online* **2**, 13.
Porat-Shliom, N., Tietgens, A. J., Van Itallie, C. M., Vitale-Cross, L., Jarnik, M., Harding, O. J., Anderson, J. M., Gutkind, J. S., Weigert, R. and Arias, I. M. (2016). Liver kinase B1 regulates hepatocellular tight junction distribution and function in vivo. *Hepatology* **64**, 1317-1329.
Powell, D., Tauzin, S., Hind, L. E., Deng, Q., Beebe, D. J. and Huttenlocher, A. (2017). Chemokine signaling and the regulation of bidirectional leukocyte migration in interstitial tissues. *Cell Rep.* **19**, 1572-1585.
Prasher, D. C., Eckenrode, V. K., Ward, W. W., Prendergast, F. G. and Cormier, M. J. (1992). Primary structure of the Aequorea victoria green-fluorescent protein. *Gene* **111**, 229-233.
Prunier, C., Josserand, V., Vollaire, J., Beerling, E., Petropoulos, C., Destaing, O., Montemagno, C., Hurbin, A., Prudent, R., de Koning, L. et al. (2016). LIM kinase inhibitor Pyr1 reduces the growth and metastatic load of breast cancers. *Cancer Res.* **76**, 3541-3552.
Qi, S., Li, H., Lu, L., Qi, Z., Liu, L., Chen, L., Shen, G., Fu, L., Luo, Q. and Zhang, Z. (2016). Long-term intravital imaging of the multicolor-coded tumor microenvironment during combination immunotherapy. *Elife* **5**, e14756.
Radbruch, H., Bremer, D., Mothes, R., Günther, R., Rinnenthal, J. L., Pohlan, J., Ulbricht, C., Hauser, A. E. and Niesner, R. (2015). Intravital FRET: probing cellular and tissue function in vivo. *Int. J. Mol. Sci.* **16**, 11713-11727.

Raposo, G. and Stoorvogel, W. (2013). Extracellular vesicles: exosomes, microvesicles, and friends. *J. Cell Biol.* **200**, 373-383.
Rapsomaniki, M. A., Kotsantis, P., Symeonidou, I.-E., Giakoumakis, N.-N., Taraviras, S. and Lygerou, Z. (2012). easyFRAP: an interactive, easy-to-use tool for qualitative and quantitative analysis of FRAP data. *Bioinformatics* **28**, 1800-1801.
Rehberg, M., Krombach, F., Pohl, U. and Dietzel, S. (2010). Signal improvement in multiphoton microscopy by reflection with simple mirrors near the sample. *J. Biomed. Opt.* **15**, 026017.
Renz, M. and Langowski, J. (2008). Dynamics of the CapG actin-binding protein in the cell nucleus studied by FRAP and FCS. *Chromosome Res.* **16**, 427-437.
Rezakhaniha, R., Agianniotis, A., Schrauwen, J. T. C., Griffa, A., Sage, D., Bouten, C. V. C., Van De Vosse, F. N., Unser, M. and Stergiopulos, N. (2012). Experimental investigation of collagen waviness and orientation in the arterial adventitia using confocal laser scanning microscopy. *Biomech. Model. Mechanobiol.* **11**, 461-473.
Richardson, D. S. and Lichtman, J. W. (2015). Clarifying tissue clearing. *Cell* **162**, 246-257.
Rinnenthal, J. L., Börnchen, C., Radbruch, H., Andresen, V., Mossakowski, A., Siffrin, V., Seelemann, T., Spiecker, H., Moll, I., Herz, J. et al. (2013). Parallelized TCSPC for dynamic intravital fluorescence lifetime imaging: quantifying neuronal dysfunction in neuroinflammation. *PLoS ONE* **8**, e60100.
Ritsma, L., Steller, E. J. A., Beerling, E., Loomans, C. J. M., Zomer, A., Gerlach, C., Vrisekoop, N., Seinstra, D., Van Gurp, L., Schafer, R. et al. (2012). Intravital microscopy through an abdominal imaging window reveals a pre-micrometastasis stage during liver metastasis. *Sci. Transl. Med.* **4**, 158ra145.
Ritsma, L., Vrisekoop, N. and Van Rheenen, J. (2013a). In vivo imaging and histochemistry are combined in the cryosection labelling and intravital microscopy technique. *Nat. Commun.* **4**, 2366.
Ritsma, L., Steller, E. J. A., Ellenbroek, S. I. J., Kranenburg, O., Borel Rinkes, I. H. M. and Van Rheenen, J. (2013b). Surgical implantation of an abdominal imaging window for intravital microscopy. *Nat. Protoc.* **8**, 583-594.
Ritsma, L., Ellenbroek, S. I. J., Zomer, A., Snippert, H. J., De Sauvage, F. J., Simons, B. D., Clevers, H. and Van Rheenen, J. (2014). Intestinal crypt homeostasis revealed at single-stem-cell level by in vivo live imaging. *Nature* **507**, 362-365.
Rodriguez-Tirado, C., Kitamura, T., Kato, Y., Pollard, J. W., Condeelis, J. S. and Entenberg, D. (2016). Long-term high-resolution intravital microscopy in the lung with a vacuum stabilized imaging window. *J. Vis. Exp.* **116**, e54603.
Samuel, M. S., Lourenço, F. C. and Olson, M. F. (2011). K-Ras mediated murine epidermal tumorigenesis is dependent upon and associated with elevated Rac1 activity. *PLoS ONE* **6**, e17143.
Sano, T., Kobayashi, T., Negoro, H., Sengiku, A., Hiratsuka, T., Kamioka, Y., Liou, L. S., Ogawa, O. and Matsuda, M. (2016). Intravital imaging of mouse urothelium reveals activation of extracellular signal-regulated kinase by stretch-induced intravesical release of ATP. *Physiol. Rep.* **4**, e13033.
Sanz-Moreno, V., Gaggioli, C., Yeo, M., Albrengues, J., Wallberg, F., Viros, A., Hooper, S., Mitter, R., Féral, C. C., Cook, M. et al. (2011). ROCK and JAK1 signaling cooperate to control actomyosin contractility in tumor cells and stroma. *Cancer Cell* **20**, 229-245.
Scheele, C. L. G. J., Hannezo, E., Muraro, M. J., Zomer, A., Langedijk, N. S. M., Van Oudenaarden, A., Simons, B. D. and Van Rheenen, J. (2017). Identity and dynamics of mammary stem cells during branching morphogenesis. *Nature* **542**, 313-317.
Schindelin, J., Arganda-Carreras, I., Frise, E., Kaynig, V., Longair, M., Pietzsch, T., Preibisch, S., Rueden, C., Saalfeld, S., Schmid, B. et al. (2012). Fiji: an open-source platform for biological-image analysis. *Nat. Methods* **9**, 676-682.
Secklehner, J., Lo Celso, C. and Carlin, L. M. (2017). Intravital microscopy in historic and contemporary immunology. *Immunol. Cell Biol.* **95**, 506-513.
Seong, J., Ouyang, M., Kim, T., Sun, J., Wen, P.-C., Lu, S., Zhuo, Y., Llewellyn, N. M., Schlaepfer, D. D., Guan, J.-L. et al. (2011). Detection of focal adhesion kinase activation at membrane microdomains by fluorescence resonance energy transfer. *Nat. Commun.* **2**, 406.
Serrels, A., Timpson, P., Canel, M., Schwarz, J. P., Carragher, N. O., Frame, M. C., Brunton, V. G. and Anderson, K. I. (2009). Real-time study of E-cadherin and membrane dynamics in living animals: implications for disease modeling and drug development. *Cancer Res.* **69**, 2714-2719.
Sherlock, B., Warren, S., Stone, J., Neil, M., Paterson, C., Knight, J., French, P. and Dunsby, C. (2015). Fibre-coupled multiphoton microscope with adaptive motion compensation. *Biomed. Opt. Express* **6**, 1876-1884.
Sherlock, B., Warren, S. C., Alexandrov, Y., Yu, F., Stone, J., Knight, J., Neil, M. A. A., Paterson, C., French, P. M. W. and Dunsby, C. (2017). In vivo multiphoton microscopy using a handheld scanner with lateral and axial motion compensation. *J. Biophotonics* **11**, e201700131.
Shih, C. and Qi, H. (2017). Intravital microscopy of T-B cell interactions in germinal centers. *Methods Mol. Biol.* **1623**, 73-85.
Shimozawa, T., Yamagata, K., Kondo, T., Hayashi, S., Shitamukai, A., Konno, D., Matsuzaki, F., Takayama, J., Onami, S., Nakayama, H. et al. (2013). Improving spinning disk confocal microscopy by preventing pinhole cross-talk for intravital imaging. *Proc. Natl. Acad. Sci. USA* **110**, 3399-3404.
Shirshin, E. A., Gurfinkel, Y. I., Priezzhev, A. V., Fadeev, V. V., Lademann, J. and Darvin, M. E. (2017). Two-photon autofluorescence lifetime imaging of human skin papillary dermis in vivo: assessment of blood capillaries and structural proteins localization. *Sci. Rep.* **7**, 1171.
Singh, A., Fedele, C., Lu, H., Nevalainen, M. T., Keen, J. H. and Languino, L. R. (2016). Exosome-mediated transfer of alphavbeta3 integrin from tumorigenic to nontumorigenic cells promotes a migratory phenotype. *Mol. Cancer Res.* **14**, 1136-1146.
Skala, M. C., Riching, K. M., Gendron-Fitzpatrick, A., Eickhoff, J., Eliceiri, K. W., White, J. G. and Ramanujam, N. (2007). In vivo multiphoton microscopy of NADH and FAD redox states, fluorescence lifetimes, and cellular morphology in precancerous epithelia. *Proc. Natl. Acad. Sci. USA* **104**, 19494-19499.
Song, H., Fraanje, R., Schitter, G., Kroese, H., Vdovin, G. and Verhaegen, M. (2010). Model-based aberration correction in a closed-loop wavefront-sensor-less adaptive optics system. *Opt. Express* **18**, 24070-24084.
Soulet, D., Paré, A., Coste, J. and Lacroix, S. (2013). Automated filtering of intrinsic movement artifacts during two-photon intravital microscopy. *PLoS ONE* **8**, e53942.
Steeg, P. S. (2016). Targeting metastasis. *Nat. Rev. Cancer* **16**, 201-218.
Steele, C. W., Karim, S. A., Leach, J. D. G., Bailey, P., Upstill-Goddard, R., Rishi, L., Foth, M., Bryson, S., Mcdaid, K., Wilson, Z. et al. (2016). CXCR2 inhibition profoundly suppresses metastases and augments immunotherapy in pancreatic ductal adenocarcinoma. *Cancer Cell* **29**, 832-845.
Stringari, C., Edwards, R. A., Pate, K. T., Waterman, M. L., Donovan, P. J. and Gratton, E. (2012). Metabolic trajectory of cellular differentiation in small intestine by Phasor Fluorescence Lifetime Microscopy of NADH. *Sci. Rep.* **2**, 568.
Sung, B. H., Ketova, T., Hoshino, D., Zijlstra, A. and Weaver, A. M. (2015). Directional cell movement through tissues is controlled by exosome secretion. *Nat. Commun.* **6**, 8164.
Szulczewski, J. M., Inman, D. R., Entenberg, D., Ponik, S. M., Aguirre-Ghiso, J., Castracane, J., Condeelis, J., Eliceiri, K. W. and Keely, P. J. (2016). In vivo visualization of stromal macrophages via label-free FLIM-based metabolite imaging. *Sci. Rep.* **6**, 25086.
Tabuchi, A., Mertens, M., Kuppe, H., Pries, A. R. and Kuebler, W. M. (2008). Intravital microscopy of the murine pulmonary microcirculation. *J. Appl. Physiol.* **104**, 338-346.
Tainaka, K., Kubota, S. I., Suyama, T. Q., Susaki, E. A., Perrin, D., Ukai-Tadenuma, M., Ukai, H. and Ueda, H. R. (2014). Whole-body imaging with single-cell resolution by tissue decolorization. *Cell* **159**, 911-924.
Thanabalasuriar, A., Neupane, A. S., Wang, J., Krummel, M. F. and Kubes, P. (2016). iNKT cell emigration out of the lung vasculature requires neutrophils and monocyte-derived dendritic cells in inflammation. *Cell Rep.* **16**, 3260-3272.
Timpson, P., Mcghee, E. J. and Anderson, K. I. (2011). Imaging molecular dynamics in vivo–from cell biology to animal models. *J. Cell Sci.* **124**, 2877-2890.
Tomer, R., Ye, L., Hsueh, B. and Deisseroth, K. (2014). Advanced CLARITY for rapid and high-resolution imaging of intact tissues. *Nat. Protoc.* **9**, 1682-1697.
Torcellan, T., Hampton, H. R., Bailey, J., Tomura, M., Brink, R. and Chtanova, T. (2017). In vivo photolabeling of tumor-infiltrating cells reveals highly regulated egress of T-cell subsets from tumors. *Proc. Natl. Acad. Sci. USA* **114**, 5677-5682.
Tsai, C.-K., Chen, Y.-S., Wu, P.-C., Hsieh, T.-Y., Liu, H.-W., Yeh, C.-Y., Lin, W.-L., Chia, J.-S. and Liu, T.-M. (2012). Imaging granularity of leukocytes with third harmonic generation microscopy. *Biomed. Opt. Express* **3**, 2234-2243.
Tsai, M.-R., Cheng, Y.-H., Chen, J.-S., Sheen, Y.-S., Liao, Y.-H. and Sun, C.-K. (2014). Differential diagnosis of nonmelanoma pigmented skin lesions based on harmonic generation microscopy. *J. Biomed. Opt.* **19**, 036001.
Tyas, L., Brophy, V. A., Pope, A., Rivett, A. J. and Tavaré, J. M. (2000). Rapid caspase-3 activation during apoptosis revealed using fluorescence-resonance energy transfer. *EMBO Rep.* **1**, 266-270.
Van Der Vos, K. E., Abels, E. R., Zhang, X., Lai, C., Carrizosa, E., Oakley, D., Prabhakar, S., Mardini, O., Crommentuijn, M. H. W., Skog, J. et al. (2016). Directly visualized glioblastoma-derived extracellular vesicles transfer RNA to microglia/macrophages in the brain. *Neuro Oncol.* **18**, 58-69.
Vennin, C., Herrmann, D., Lucas, M. C. and Timpson, P. (2016). Intravital imaging reveals new ancillary mechanisms co-opted by cancer cells to drive tumor progression. *F1000Res* **5**, 8090.
Vennin, C., Chin, V. T., Warren, S. C., Lucas, M. C., Herrmann, D., Magenau, A., Melenec, P., Walters, S. N., Del Monte-Nieto, G., Conway, J. R. W. et al. (2017). Transient tissue priming via ROCK inhibition uncouples pancreatic cancer progression, sensitivity to chemotherapy, and metastasis. *Sci. Transl. Med.* **9**, eaai8504.
Vercauteren, T., Perchant, A., Malandain, G., Pennec, X. and Ayache, N. (2006). Robust mosaicing with correction of motion distortions and tissue deformations for in vivo fibered microscopy. *Med. Image Anal.* **10**, 673-692.
Verma, S., Han, S. P., Michael, M., Gomez, G. A., Yang, Z., Teasdale, R. D., Ratheesh, A., Kovacs, E. M., Ali, R. G. and Yap, A. S. (2012). A WAVE2-Arp2/3 actin nucleator apparatus supports junctional tension at the epithelial zonula adherens. *Mol. Biol. Cell* **23**, 4601-4610.

Vinegoni, C., Sungon Lee, C., Feruglio, P. F. and Weissleder, R. (2014). Advanced motion compensation methods for intravital optical microscopy. *IEEE J. Sel. Top. Quantum Electron.* **20**, 83-91.
Vinegoni, C., Aguirre, A. D., Lee, S. and Weissleder, R. (2015). Imaging the beating heart in the mouse using intravital microscopy techniques. *Nat. Protoc.* **10**, 1802-1819.
Wagner, S., Chiosea, S., Ivshina, M. and Nickerson, J. A. (2004). In vitro FRAP reveals the ATP-dependent nuclear mobilization of the exon junction complex protein SRm160. *J. Cell Biol.* **164**, 843-850.
Walsh, A. J., Cook, R. S., Manning, H. C., Hicks, D. J., Lafontant, A., Arteaga, C. L. and Skala, M. C. (2013). Optical metabolic imaging identifies glycolytic levels, subtypes, and early-treatment response in breast cancer. *Cancer Res.* **73**, 6164-6174.
Wang, Y., Botvinick, E. L., Zhao, Y., Berns, M. W., Usami, S., Tsien, R. Y. and Chien, S. (2005). Visualizing the mechanical activation of Src. *Nature* **434**, 1040-1045.
Wang, X., He, L., Wu, Y. I., Hahn, K. M. and Montell, D. J. (2010). Light-mediated activation reveals a key role for Rac in collective guidance of cell movement in vivo. *Nat. Cell Biol.* **12**, 591-597.
Wang, C., Liu, R., Milkie, D. E., Sun, W., Tan, Z., Kerlin, A., Chen, T.-W., Kim, D. S. and Ji, N. (2014). Multiplexed aberration measurement for deep tissue imaging in vivo. *Nat. Methods* **11**, 1037-1040.
Wang, M., Tang, F., Pan, X., Yao, L., Wang, X., Jing, Y., Ma, J., Wang, G. and Mi, L. (2017). Rapid diagnosis and intraoperative margin assessment of human lung cancer with fluorescence lifetime imaging microscopy. *BBA Clin.* **8**, 7-13.
Warren, S. C., Margineanu, A., Alibhai, D., Kelly, D. J., Talbot, C., Alexandrov, Y., Munro, I., Katan, M., Dunsby, C. and French, P. M. W. (2013). Rapid global fitting of large fluorescence lifetime imaging microscopy datasets. *PLoS ONE* **8**, e70687.
Weigelin, B., Bakker, G.-J. and Friedl, P. (2012). Intravital third harmonic generation microscopy of collective melanoma cell invasion. *IntraVital* **1**, 32-43.
Weigelin, B., Bolaños, E., Teijeira, A., Martinez-Forero, I., Labiano, S., Azpilikueta, A., Morales-Kastresana, A., Quetglas, J. I., Wagena, E., Sánchez-Paulete, A. R. et al. (2015). Focusing and sustaining the antitumor CTL effector killer response by agonist anti-CD137 mAb. *Proc. Natl. Acad. Sci. USA* **112**, 7551-7556.
Weitsman, G., Barber, P. R., Nguyen, L. K., Lawler, K., Patel, G., Woodman, N., Kelleher, M. T., Pinder, S. E., Rowley, M., Ellis, P. A. et al. (2016). HER2-HER3 dimer quantification by FLIM-FRET predicts breast cancer metastatic relapse independently of HER2 IHC status. *Oncotarget* **7**, 51012-51026.
Williams, E., Moore, J., Li, S. W., Rustici, G., Tarkowska, A., Chessel, A., Leo, S., Antal, B., Ferguson, R. K., Sarkans, U. et al. (2017). Image data resource: a bioimage data integration and publication platform. *Nat. Methods* **14**, 775-781.
Xu, H., Li, X., Liu, D., Li, J., Zhang, X., Chen, X., Hou, S., Peng, L., Xu, C., Liu, W. et al. (2013a). Follicular T-helper cell recruitment governed by bystander B cells and ICOS-driven motility. *Nature* **496**, 523-527.
Xu, X., Cheng, J., Thrall, M. J., Liu, Z., Wang, X. and Wong, S. T. C. (2013b). Multimodal non-linear optical imaging for label-free differentiation of lung cancerous lesions from normal and desmoplastic tissues. *Biomed. Opt. Express* **4**, 2855-2868.
Yamada, S., Pokutta, S., Drees, F., Weis, W. I. and Nelson, W. J. (2005). Deconstructing the cadherin-catenin-actin complex. *Cell* **123**, 889-901.
Yamaguchi, Y., Shinotsuka, N., Nonomura, K., Takemoto, K., Kuida, K., Yosida, H. and Miura, M. (2011). Live imaging of apoptosis in a novel transgenic mouse highlights its role in neural tube closure. *J. Cell Biol.* **195**, 1047-1060.
Yan, X. J., Wu, G. Q., Qu, Q. R., Fan, X. B., Xu, X. D. and Liu, N. F. (2016). A hybrid peptide PTS that facilitates transmembrane delivery and its application for the rapid in vivo imaging via near-infrared fluorescence imaging. *Front. Pharmacol.* **7**, 00051.
Yang, Z., Xie, W., Ju, F., Khan, A. and Zhang, S. (2017). In vivo two-photon imaging reveals a role of progesterone in reducing axonal dieback after spinal cord injury in mice. *Neuropharmacology* **116**, 30-37.
Yokoi, A., Yoshioka, Y., Yamamoto, Y., Ishikawa, M., Ikeda, S.-I., Kato, T., Kiyono, T., Takeshita, F., Kajiyama, H., Kikkawa, F. et al. (2017). Malignant extracellular vesicles carrying MMP1 mRNA facilitate peritoneal dissemination in ovarian cancer. *Nat. Commun.* **8**, 14470.
Yu, T., Qi, Y., Gong, H., Luo, Q. and Zhu, D. (2017). Optical clearing for multi-scale biological tissues. *J. Biophotonics* **11**, 201700187.
Zenaro, E., Rossi, B., Angiari, S. and Constantin, G. (2013). Use of imaging to study leukocyte trafficking in the central nervous system. *Immunol. Cell Biol.* **91**, 271-280.
Zhao, Z., Zhu, X., Cui, K., Mancuso, J., Federley, R., Fischer, K., Teng, G., Mittal, V., Gao, D., Zhao, H. et al. (2016). In vivo visualization and characterization of epithelial-mesenchymal transition in breast tumors. *Cancer Res.* **76**, 2094-2104.
Zipfel, W. R., Williams, R. M., Christie, R., Nikitin, A. Y., Hyman, B. T. and Webb, W. W. (2003). Live tissue intrinsic emission microscopy using multiphoton-excited native fluorescence and second harmonic generation. *Proc. Natl. Acad. Sci. USA* **100**, 7075-7080.
Zomer, A., Maynard, C., Verweij, F. J., Kamermans, A., Schäfer, R., Beerling, E., Schiffelers, R. M., de Wit, E., Berenguer, J., Ellenbroek, S. I. J. et al. (2015). In Vivo imaging reveals extracellular vesicle-mediated phenocopying of metastatic behavior. *Cell* **161**, 1046-1057.